Feeding induces cholesterol biosynthesis via the mTORC1–USP20–HMGCR axis

https://doi.org/10.1038/s41586-020-2928-y

Received: 13 November 2019

Accepted: 19 August 2020

Published online: 11 November 2020

Check for updates

Xiao-Yi Lu[1,3], Xiong-Jie Shi[1,3], Ao Hu[1,3], Ju-Qiong Wang[1,3], Yi Ding[1], Wei Jiang[1], Ming Sun[1], Xiaolu Zhao[1], Jie Luo[1], Wei Qi[2] & Bao-Liang Song[1]✉

Cholesterol is an essential lipid and its synthesis is nutritionally and energetically costly[1,2]. In mammals, cholesterol biosynthesis increases after feeding and is inhibited under fasting conditions[3]. However, the regulatory mechanisms of cholesterol biosynthesis at the fasting–feeding transition remain poorly understood. Here we show that the deubiquitylase ubiquitin-specific peptidase 20 (USP20) stabilizes HMG-CoA reductase (HMGCR), the rate-limiting enzyme in the cholesterol biosynthetic pathway, in the feeding state. The post-prandial increase in insulin and glucose concentration stimulates mTORC1 to phosphorylate USP20 at S132 and S134; USP20 is recruited to the HMGCR complex and antagonizes its degradation. The feeding-induced stabilization of HMGCR is abolished in mice with liver-specific *Usp20* deletion and in USP20(S132A/S134A) knock-in mice. Genetic deletion or pharmacological inhibition of USP20 markedly decreases diet-induced body weight gain, reduces lipid levels in the serum and liver, improves insulin sensitivity and increases energy expenditure. These metabolic changes are reversed by expression of the constitutively stable HMGCR(K248R). This study reveals an unexpected regulatory axis from mTORC1 to HMGCR via USP20 phosphorylation and suggests that inhibitors of USP20 could be used to lower cholesterol levels to treat metabolic diseases including hyperlipidaemia, liver steatosis, obesity and diabetes.

Cholesterol has multiple physiological roles, including modulation of membrane function, serving as a precursor to bile acids and steroid hormones[1], and covalently modifying hedgehog and smoothened proteins[1,4–6]. High levels of cholesterol and other lipids are major risk factors for cardiovascular disease, nonalcoholic fatty liver disease, obesity and diabetes[7].

A human adult needs about 1 g of cholesterol per day, either from de novo biosynthesis or from intestinal absorption[2]. The liver is the major cholesterol biosynthetic organ. Cholesterol is synthesized from acetyl-CoA through about 30 steps. HMGCR converts HMG-CoA to mevalonate[8] and is the rate-limiting enzyme in cholesterol biosynthesis. Cholesterol biosynthesis is stringently regulated to prevent toxicity caused by excess cholesterol. This regulation occurs mainly through two negative-feedback pathways, sterol-induced degradation of HMGCR and sterol-regulated processing of sterol regulatory element-binding proteins (SREBPs), which govern the transcription of all cholesterogenic genes[9,10]. However, animals have adapted to an inconsistent food supply and cycles of famine (fasting) and feasting (feeding)[11]. It is well established that cholesterol biosynthesis is repressed in the fasting state and increases upon feeding[3]. However, the mechanism is not well defined.

Feeding induces HMGCR expression

To investigate the regulatory mechanism of cholesterol biosynthesis in fasting and refeeding conditions, we measured the expression of cholesterogenic enzymes including HMGCR, farnesyl diphosphate farnesyltransferase 1 (FDFT1), lanosterol synthase (LSS) and 24-dehydrocholesterol reductase (DHCR24) in the liver. After overnight fasting, mice were fed a high-sucrose, low-fat diet with little cholesterol to eliminate interference from feedback regulation. The level of HMGCR protein was increased by about 20-fold upon refeeding (Fig. 1a, Extended Data Fig. 1a–d), whereas levels of FDFT1, LSS and DHCR24 were increased by less than 1-fold (Fig. 1a). The messenger RNAs encoding these proteins were increased by two- to fourfold (Extended Data Fig. 1b, e). These results suggest that the induction of HMGCR protein following feeding involves a post-transcriptional mechanism in addition to the well-characterized transcriptional regulation[1].

When sterol levels are high, HMGCR is ubiquitinated by the E3 ligase gp78 and targeted for degradation[12–14]. We evaluated whether this mechanism targets HMGCR for degradation in starved and refed mice using an in vitro ubiquitination system[12,15,16] (Extended Data Fig. 1f, g). As a positive control, we increased HMGCR ubiquitination using 25-hydroxycholesterol (25-HC) (Extended Data Fig. 1g). We observed much higher HMGCR ubiquitination with liver cytosol from fasted mice than from refed mice (Extended Data Fig. 1g), suggesting two possibilities: the fasted liver cytosol contains factor(s) that enhance the E3 activity, or the refed liver cytosol contains higher deubiquitylase (DUB) activity. We next performed an in vitro deubiquitination assay to distinguish between these possibilities (Fig. 1b). We immunoprecipitated

[1]Hubei Key Laboratory of Cell Homeostasis, College of Life Sciences, Frontier Science Center for Immunology and Metabolism, the Institute for Advanced Studies, Wuhan University, Wuhan, China. [2]School of Life Science and Technology, ShanghaiTech University, Shanghai, China. [3]These authors contributed equally: Xiao-Yi Lu, Xiong-Jie Shi, Ao Hu, Ju-Qiong Wang. ✉e-mail: blsong@whu.edu.cn

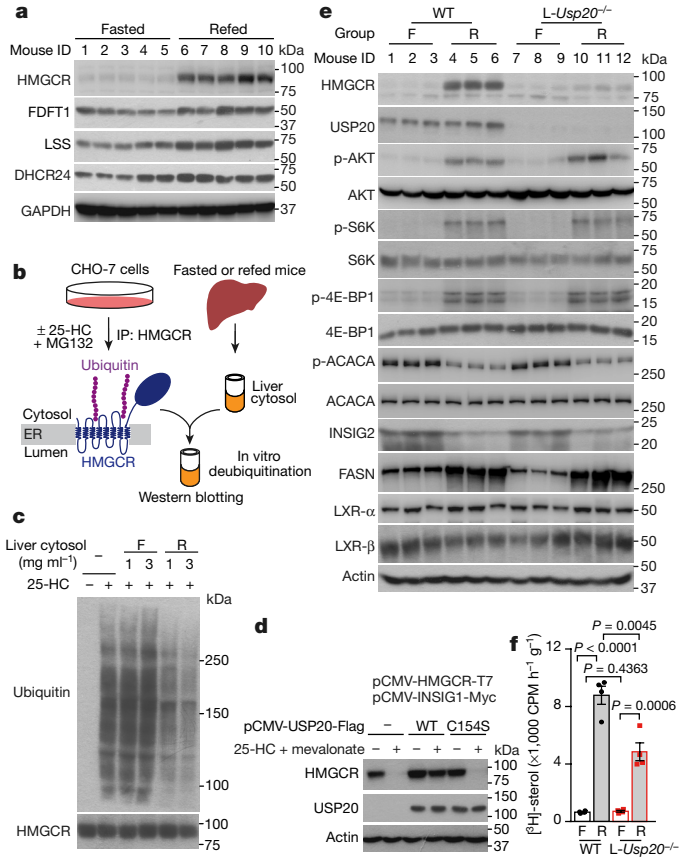

Fig. 1 | USP20 is required for feeding-induced increase of HMGCR. **a**, Immunoblot analysis of liver samples. Eight-week-old male mice were fasted for 12 h, or fasted for 12 h and then refed a high-carbohydrate, low-fat diet for 12 h ($n = 5$ per group). **b**, Schematic representation of in vitro deubiquitination assay. The ubiquitinated HMGCR was immunoprecipitated (IP) from sterol-treated CHO-7 cells, incubated with liver cytosol fractions and analysed by immunoblotting. ER, endoplasmic reticulum. **c**, In vitro deubiquitination analysis of HMGCR as performed in **b**. **d**, Requirement for the catalytic activity of USP20 to stabilize HMGCR. Huh7 cells were transfected with the indicated plasmids, depleted of sterols and treated with 25-HC and mevalonate for 5 h. The cells were collected and analysed by immunoblotting. Experiments in **c**, **d**, were performed as indicated three times with similar results. **e**, Eight-week-old male L-*Usp20*$^{-/-}$ mice and their wild-type (WT) littermates ($n = 3$ per group) were subjected to fasting and refeeding protocols and liver samples were analysed by immunoblotting. F, fasted; R, refed. **f**, Incorporation of tritium-labelled water into sterol in liver of wild-type and L-*Usp20*$^{-/-}$ male mice ($n = 4$ per group). Data are mean ± s.e.m.; unpaired two-tailed Student's *t*-test.

ubiquitinated HMGCR from CHO-7 cells treated with 25-HC (to stimulate HMGCR ubiquitination) and MG132 (to block protein degradation)[17], and then incubated the immunoprecipitate with cytosol from liver (Fig. 1b). HMGCR ubiquitination was unchanged in the presence of fasted liver cytosol, but was substantially decreased by the refed liver cytosol (Fig. 1c). Together, these results suggest that the liver of refed mice contains higher DUB activity, which protects HMGCR from ubiquitin-mediated proteasomal degradation.

Feeding-induced HMGCR requires USP20

There are about 90 DUBs in the human genome[18]. We co-expressed individual DUBs with HMGCR and INSIG1[19] in a screen for the blocker of HMGCR degradation. USP20 was the only positive hit in the screen (Extended Data Fig. 2). In contrast to wild-type USP20, the enzymatically inactive USP20(C154S) did not stabilize HMGCR (Fig. 1d). USP20 preferentially hydrolyzed K48- and K63-linkages and reduced HMGCR ubiquitination, which was inhibited by the USP20-specific inhibitor GSK2643943A (Extended Data Fig. 3a–e). Conversely, knockdown of *USP20* accelerated HMGCR degradation (Extended Data Fig. 3f–i).

USP20 was highly expressed in liver (Extended Data Fig. 4a), suggesting a potential role in hepatic function. We generated liver-specific *Usp20*-deficient mice (L-*Usp20*$^{-/-}$) (Extended Data Fig. 4b–f). Refeeding markedly increased HMGCR protein level in wild-type, but not in L-*Usp20*$^{-/-}$ liver (Fig. 1e). The levels of phosphorylated AKT (p-AKT), p-S6K, p-4E-BP1, p-ACACA, INSIG2 and fatty acid synthase (FASN) in response to fasting–refeeding transition were similar in both genotypes (Fig. 1e). We next measured the de novo cholesterol biosynthesis by analysing the incorporation of ^{3}H-labelled H_2O. Refeeding increased cholesterol synthesis by 12.4-fold in wild-type liver, but this effect was reduced by 45% in L-*Usp20*$^{-/-}$ liver (Fig. 1f). Kidney cholesterol synthesis remained unchanged (Extended Data Fig. 4g). These results indicate that USP20 is the feeding-responsive liver HMGCR deubiquitylase, and its ablation does not affect the insulin- and glucose-signalling pathways.

Notably, circulating lipid and glucose levels were significantly lower in L-*Usp20*$^{-/-}$ mice than in wild-type mice (Extended Data Fig. 4h). The transcripts of cholesterogenic genes were similarly expressed in wild-type and L-*Usp20*$^{-/-}$ mice (Extended Data Fig. 4i); however, expression of *Srebp1c* and fatty acid biosynthetic genes was decreased in L-*Usp20*$^{-/-}$ mice in the refed state. Levels of liver X receptor- α (LXRα) and LXRβ proteins were unaltered in wild-type and L-*Usp20*$^{-/-}$ in starved and refed states (Fig. 1e), whereas their target genes were downregulated in L-*Usp20*$^{-/-}$ mice (Extended Data Fig. 4i). This may result from decreased production of sterols (Fig. 1f), which activate LXR and downstream expression of *Srebp1c* and other target genes[20,21].

Insulin and glucose regulate USP20 function

We next sought to identify the feeding signal that mediates USP20-stabilization of HMGCR. As the most marked changes after feeding occurred in circulating glucose and insulin[22], we fasted wild-type mice overnight and intraperitoneally injected them with glucose or insulin. Liver HMGCR expression was synergistically elevated by glucose and insulin, whereas USP20 levels remained constant (Extended Data Fig. 4j, k). Insulin and glucose substantially increased the HMGCR protein level in wild-type, but not in *Usp20*-deficient hepatocytes, although there were no differences in signalling molecules such as p-AKT, p-S6K, p-4E-BP1 and p-ACACA (Fig. 2a, Extended Data 4l, m).

The insulin signalling cascade involves PI3K, AKT and mTOR[23], whereas AMPK inhibits mTORC1 activity at low glucose[24–28]. Wortmannin (a PI3K inhibitor), AKTi-1/2 (an AKT inhibitor) and rapamycin (an mTORC1 inhibitor)[23] all abrogated USP20-mediated accumulation of HMGCR (Extended Data Fig. 4n). Conversely, the AMPK inhibitor dorsomorphin restored HMGCR stabilization by USP20 in low-glucose conditions (Extended Data Fig. 4o), whereas the AMPK activator A-769662 abolished USP20-mediated stabilization of HMGCR in high-glucose conditions (Extended Data Fig. 4p). Thus, USP20 probably responds to insulin and glucose downstream of mTORC1.

mTORC1 phosphorylates USP20 at S132 and S134

Quantitative mass spectrometry identified several differentially phosphorylated peptides of USP20. Phosphorylation at Ser132 and Ser134 residues was detected only in the high-glucose condition (Extended Data Fig. 5a–d), as reported in previous mTORC1 phosphoproteomics studies[29,30]. We used an antibody specific for phosphorylated Ser132 and Ser134 of USP20 (p-USP20) (Extended Data Fig. 5e) and showed that USP20 was effectively phosphorylated by immunoprecipitated mTORC1 but not mTORC2 in vitro, and the mTOR inhibitor torin1 blocked the phosphorylation (Fig. 2b). USP20(S132A/S134A) was not phosphorylated by mTORC1 (Fig. 2c). Rapamycin inhibited the

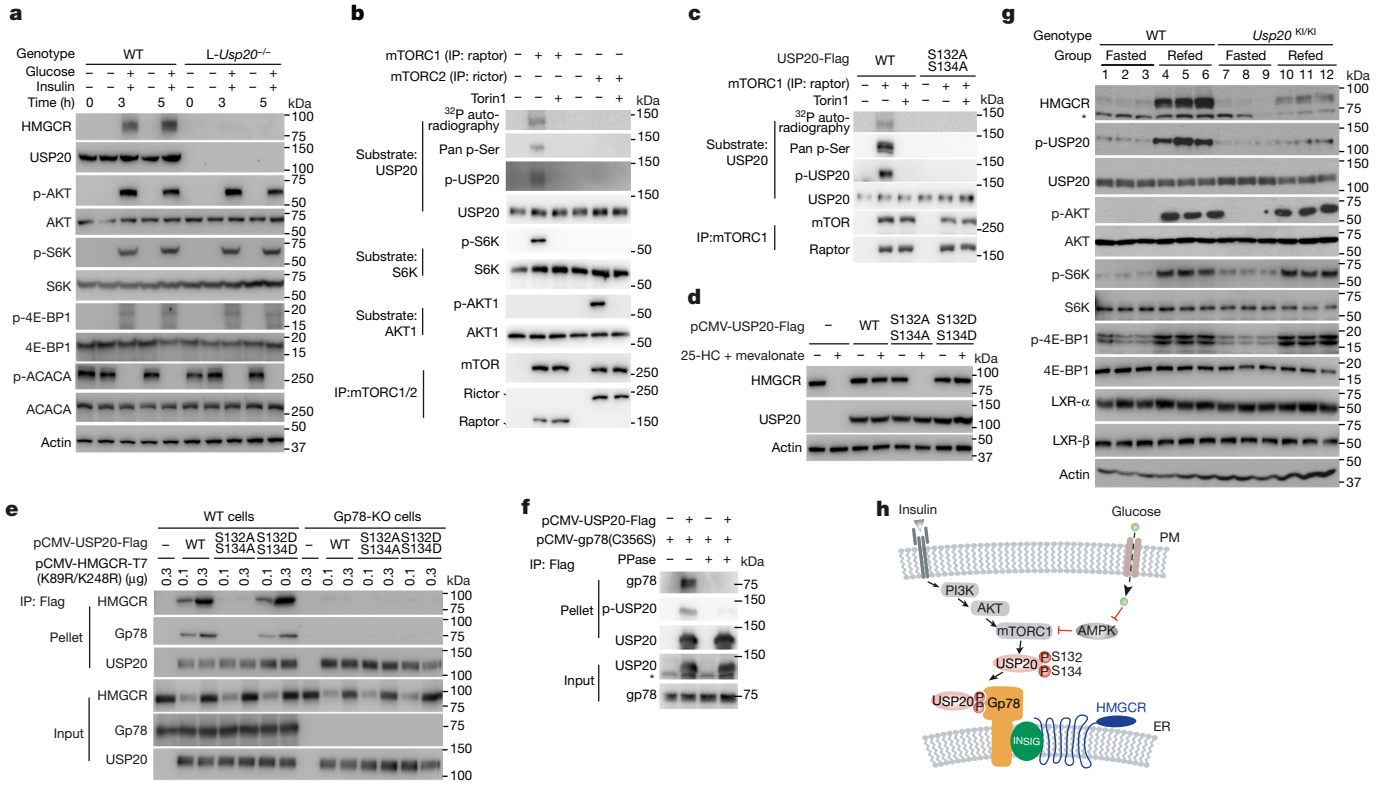

Fig. 2 | Insulin and glucose regulate USP20 through mTORC1-mediated phosphorylation at S132 and S134. a, Primary hepatocytes from wild-type and L-*Usp20*$^{-/-}$ mice were cultured in M199 medium (containing 5.5 mM glucose) and were untreated or treated with an additional 20 mM glucose with or without 10 nM insulin. After 3 h or 5 h, cells were collected and analysed by immunoblotting. **b**, mTORC1 phosphorylates USP20 in vitro. The reaction was primed with the addition of 100 μM cold ATP (or ATP containing an additional 10 μCi per tube of [γ-^{32}P]-ATP for autoradiography of USP20). The reaction was immunoblotted with a pan-anti-phospho-Ser antibody, anti-phosphorylated USP20 Ser132 and Ser134 (p-USP20) and other antibodies as indicated. **c**, mTORC1 phosphorylates USP20 at S132 and S134 in vitro. The immunopurified wild-type USP20–Flag or USP20(S132A/S134A)–Flag proteins were incubated with mTORC1 in vitro and analysed as in **b**. **d**, Phosphorylation of USP20 S132 and S134 is required for HMGCR stabilization. Huh7 cells were co-transfected with the indicated USP20 plasmids with plasmids encoding HMGCR and INSIG1, depleted of sterols and treated with 25-HC and mevalonate for 5 h. The cells were collected and analysed by immunoblotting. **e**, The wild-type and *Gp78*-knockout (KO) cells were transfected with the indicated plasmids. USP20 was immunoprecipitated with anti-Flag beads. **f**, Dephosphorylation of USP20 abolishes its interaction with gp78. Cells were transfected with the indicated plasmids. The cell lysates were incubated with calf intestinal phosphatase and λ phosphatase (PPase) for 30 min, and immunoprecipitated with anti-Flag beads. Gp78(C356S) has no E3 activity. Experiments in **a**–**f** were repeated twice with similar results. **g**, Immunoblot analysis of liver lysates. Eight-week-old male *Usp20*$^{KI/KI}$ mice and their male wild-type littermates ($n = 3$ per group) were subjected to fasting and refeeding. Asterisk indicates nonspecific band. **h**, A simplified model depicting the regulatory mechanism of USP20 by insulin and glucose signalling pathways. The active mTORC1 phosphorylates USP20 at S132 and S134, which promotes the interaction with gp78, stabilizing HMGCR. ER, endoplasmic reticulum; PM, plasma membrane.

phosphorylation of USP20 in cells and refed mouse liver (Extended Data Fig. 5f, g) and counteracted feeding-induced increases of HMGCR and serum lipid levels (Extended Data Fig. 5g–k).

The phosphorylation-null USP20(S132A/134A) and phosphomimetic USP20(S132D/S134D) exhibited similar DUB activities to wild-type USP20 in vitro (Extended Data Fig. 5l). However, unlike wild-type USP20 and USP20(S132D/S134D), USP20(S132A/134A) did not antagonize sterol-induced degradation of HMGCR (Fig. 2d). HMGCR interacted with wild-type USP20 and USP20(S132D/S134D) but not USP20(S132A/S134A) (Fig. 2e). This interaction was completely absent in cells deficient in *Gp78* (also known as *Amfr*)[14] (Fig. 2e), suggesting that gp78 may bridge the interaction between USP20 and HMGCR. Indeed, gp78 interacted with USP20 regardless of sterol levels, and the region of gp78 including residues 383–578 was required for USP20 binding (Extended Data Fig. 5m–q). Moreover, phosphatase treatment largely diminished the phosphorylation of USP20 and USP20–gp78 interaction (Fig. 2f).

Next, we generated USP20(S132A/S134A) knock-in (*Usp20*$^{KI/KI}$) mice (Extended Data Fig. 6a). Upon refeeding, hepatic HMGCR levels were markedly increased in wild-type mice, but only slightly increased in the *Usp20*$^{KI/KI}$ mice (Fig. 2g). Feeding-induced phosphorylation of USP20 at S132/S134 was also abolished in *Usp20*$^{KI/KI}$ mice (Fig. 2g). *Usp20*$^{KI/KI}$ mice displayed lower lipid levels than wild-type mice and a similar hepatic gene expression profile to that of L-*Usp20*$^{-/-}$ mice (Extended Data Figs. 4i, 6b–g). Unlike liver cytosol from refed wild-type mice, liver cytosol from L-*Usp20*$^{-/-}$, *Usp20*$^{KI/KI}$ or rapamycin-treated wild-type mice did not cause cleavage of ubiquitin chains from HMGCR (Extended Data Fig. 6h, i).

Thus, we proposed the working model shown in Fig. 2h: feeding-induced insulin- and glucose-signalling pathways activate mTORC1, which phosphorylates USP20 at S132 and S134. The phosphorylated USP20 then binds gp78 and stabilizes HMGCR by deubiquitination, thereby increasing cholesterol biosynthesis in the liver.

Metabolic profile of L-*Usp20*$^{-/-}$ mice

To further investigate the function of USP20 in metabolic diseases, we fed mice with a high-fat and high-sucrose (HFHS) diet. Compared with WT mice, L-*Usp20*$^{-/-}$ mice showed similar cumulative food intake and nutrient absorption but gained less body weight (Fig. 3a, Extended Data Fig. 6j–l). L-*Usp20*$^{-/-}$ mice exhibited similar lean mass to body weight ratio, but less fat accumulation in liver and white adipose tissue (WAT) (Fig. 3b–f), and lower cholesterol and triglycerides levels in all

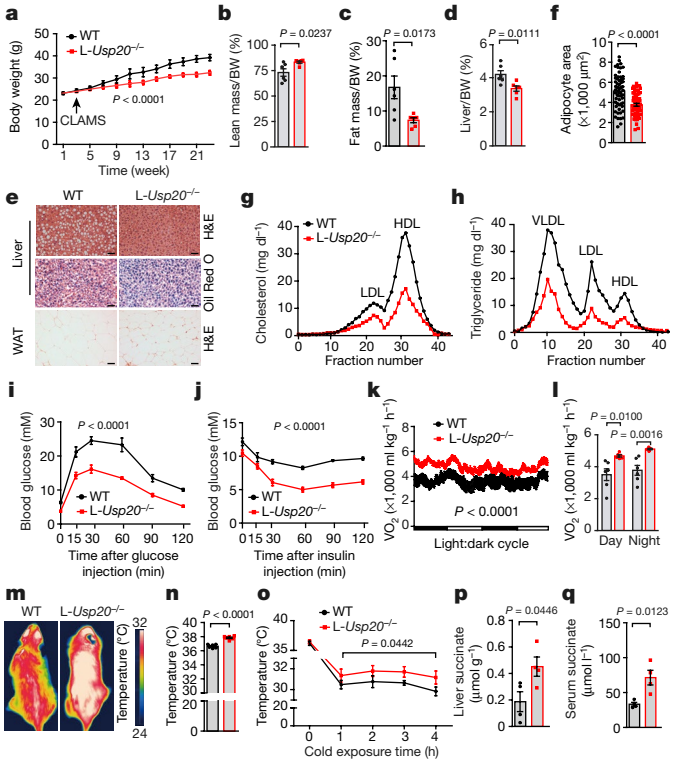

Fig. 3 | L-*Usp20*$^{-/-}$ mice display improved metabolism. Eight-week-old male L-*Usp20*$^{-/-}$ mice and their male wild-type littermates were randomly grouped ($n = 6$ per group) and allowed ad libitum access to water and HFHS diet for 23 weeks. **a**, Body weight. **b**, **c**, Whole-body composition of the mice after 23 weeks of HFHS feeding. BW, body weight. **d**, Liver as a proportion of body weight of the mice after 23 weeks of HFHS feeding. **e**, Liver and WAT sections were stained with haematoxylin and eosin (H&E) or oil red O. Scale bars, 50 μm. **f**, Quantification of the individual adipocyte size in **e**. Sixty arbitrarily chosen adipocytes were analysed by ImageJ. **g**, **h**, Lipoprotein profiling analysis of cholesterol and triglycerides in serum by fast protein liquid chromatography. HDL, high-density lipoprotein; LDL, low-density lipoprotein; VLDL, very-low-density lipoprotein. **i**, **j**, Glucose tolerance test and insulin tolerance test performed after eight weeks of HFHS feeding. **k**, **l**, Whole-body oxygen consumption measured after three weeks of HFHS feeding. **m**, Representative infrared thermal images to measure temperature of body surface. **n**, Rectal temperature of the mice. **o**, Rectal temperature of the mice at different times after cold exposure (4 °C). **p**, **q**, Succinate levels in the liver and serum. Data are mean ± s.e.m. Statistical significance was determined using unpaired two-tailed Student's *t*-test (**b**–**d**, **f**, **l**, **n**, **p**, **q**) or two-way analysis of variance (ANOVA) (**a**, **i**–**k**, **o**).

lipoprotein fractions (Fig. 3g, h). Furthermore, glucose clearance and insulin sensitivity were substantially improved in L-*Usp20*$^{-/-}$ mice (Fig. 3i, j). The *Usp20*$^{KI/KI}$ mice showed a similar trend (Extended Data Fig. 6o–u). After three weeks of HFHS feeding, before the differences in body weight occurred, L-*Usp20*$^{-/-}$ mice exhibited significantly increased oxygen consumption and energy expenditure (Fig. 3k, l), but no differences in respiratory exchange ratio and physical activity (Extended Data Fig. 6m, n). Indeed, L-*Usp20*$^{-/-}$ mice displayed higher body temperature than wild-type mice (Fig. 3m–o); this increased energy expenditure provides a mechanistic explanation for the lower gain in body weight and other metabolic differences in these mice when maintained on the HFHS diet.

Mice on long-term HFHS diet develop metabolic diseases. Compared with chow diet, chronic HFHS diet increased AKT–mTORC1 signalling and reduced AMPK activity in both wild-type and L-*Usp20*$^{-/-}$ mice (Extended Data Fig. 6v, w). Phosphorylation of USP20 at S132 and S134 was markedly increased and levels of HMGCR were elevated in wild-type mice, but not in L-*Usp20*$^{-/-}$ mice on the HFHS diet compared with those on the chow diet (Extended Data Fig. 6v, w). Although both chow-fed and HFHS-fed wild-type mice remained responsive to the fasting–refeeding paradigm, refeeding induced much higher mTORC1 signalling and higher HMGCR level in the HFHS-fed group (Extended Data Fig. 6w). These results suggest that long-term HFHS diet chronically activates mTORC1, increasing HMGCR level by phosphorylating USP20 and exacerbating metabolic diseases.

To investigate whether destabilization of HMGCR is critical for the phenotypes of L-*Usp20*$^{-/-}$ mice, we used adeno-associated virus serotype 8 (AAV8) to express HMGCR(K248R), a HMGCR mutant resistant to sterol-induced degradation[19] or USP20-mediated stabilization, in mouse liver (Extended Data Fig. 7a–c). AAV-HMGCR(K248R) expression abolished the improvement of body weight, serum total cholesterol and triglyceride of L-*Usp20*$^{-/-}$ mice (Extended Data Fig. 7d–f). The enhanced energy expenditure and glucose clearance in L-*Usp20*$^{-/-}$ mice were also reversed by expression of HMGCR(K248R) (Extended Data Fig. 7g–i). We next generated HMGCR(K248R) knock-in mice (*Hmgcr*$^{KI/KI}$) (Extended Data Fig. 7j) and crossed them with L-*Usp20*$^{-/-}$. In contrast to wild-type HMGCR, HMGCR(K248R) was refractory to fasting–refeeding regulation and was unaffected by *Usp20* deficiency (Extended Data Fig. 7k). The lower serum lipid levels, increased energy expenditure and increased glucose clearance in L-*Usp20*$^{-/-}$ mice were reversed by HMGCR(K248R) knock-in (Extended Data Fig. 7l–p).

We next investigated the mechanism underlying increased energy expenditure in L-*Usp20*$^{-/-}$ mice. USP20 deficiency accelerates degradation of HMGCR, which may cause accumulation of HMG-CoA, which can be cleaved by HMG-CoA lyase to make acetoacetate[31]. Acetoacetate, together with succinyl-CoA, is converted to succinate and acetoacetate-CoA by succinyl-CoA: 3-oxoacid CoA transferase[32] (Extended Data Fig. 8a), and succinate is known to activate thermogenesis[33,34]. We found 67% higher levels of HMG-CoA in liver of L-*Usp20*$^{-/-}$ mice compared with wild-type mice. Acetoacetate was also increased in liver of L-*Usp20*$^{-/-}$ mice, albeit not significantly, whereas succinyl-CoA was decreased by about 44% and succinate was increased by 1.4-fold in L-*Usp20*$^{-/-}$ liver (Fig. 3p, Extended Data Fig. 8b, c). Consistently, serum succinate level was doubled in L-*Usp20*$^{-/-}$ mice compared with wild-type mice (Fig. 3q). Other intermediates in the tricarboxylic acid cycle and several known thermogenic factors were not substantially different in L-*Usp20*$^{-/-}$ mice and no liver damage was detected (Extended Data Fig. 8c–l). Together, these data indicate that hepatic ablation of *Usp20* decreases HMGCR, which feeds back to increase succinate that subsequently stimulates thermogenesis.

Effects of the USP20 inhibitor

The specific USP20 inhibitor GSK2643943A can be used to study the effect of pharmacological inhibition of USP20 in vivo[35] (Extended Data Fig. 9a, b). The induction of HMGCR by refeeding was abrogated by GSK2643943A, with no effect on the levels of phosphorylated and total USP20 (Fig. 4a, b). GSK2643943A reduced cholesterol biosynthesis by about 50% in the feeding state (Fig. 4c). Concordantly, GSK2643943A treatment decreased serum lipid contents (Extended Data Fig. 9c, d), improved glucose clearance and increased succinate levels and energy expenditure (Fig. 4d, e, Extended Data Fig. 8e–i).

We investigated whether GSK2643943A could be used to treat diet-induced obesity and obesity-related disorders. Wild-type mice were fed the HFHS diet for 15 weeks to induce obesity, and then given vehicle or GSK2643943A by oral gavage for 2 weeks (Fig. 4f). Pharmacological inhibition of USP20 did not affect food consumption or nutrient absorption (Extended Data Fig. 9j, k), but gradually decreased body weight (Fig. 4g), mainly by reducing the fat mass (Extended Data Fig. 9l–q). Lipid levels in liver, serum and adipocytes were markedly decreased following treatment with GSK2643943A (Fig. 4h–m). GSK2643943A-treated mice displayed higher energy expenditure and improved glucose clearance compared with control mice (Fig. 4n,

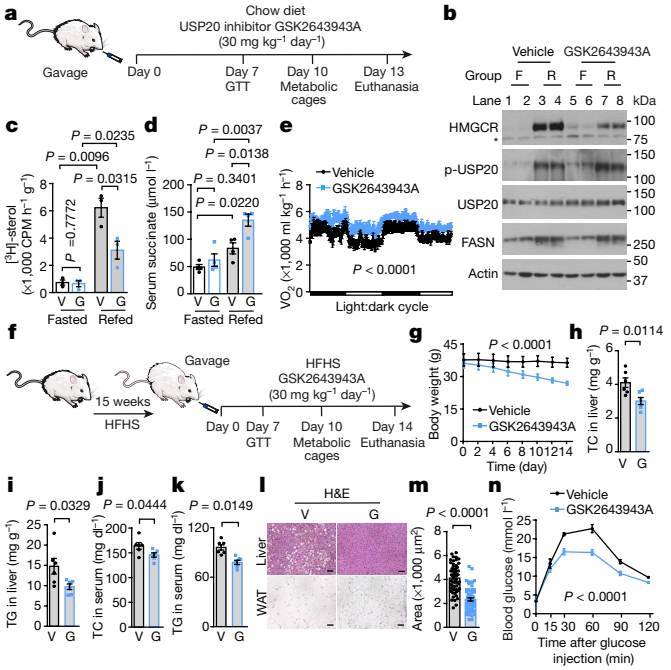

Fig. 4 | Pharmacological USP20 inhibition improves metabolism in mice. **a**, Schematic of treatment with the USP20 inhibitor GSK2643943A. Eight-week-old male C57BL/6J mice on a chow diet were gavaged with 0 or 30 mg kg^{-1} GSK2643943A daily for 13 days. **b**, After 13 days of GSK2643943A treatment, mice were subjected to fasting and refeeding. Liver samples were analysed by immunoblotting. Experiments were performed as indicated twice with similar results. **c**, Incorporation of tritium-labelled water into sterol in the liver of male mice gavaged with vehicle or GSK2643943A ($n = 3$ per group). **d**, Succinate levels in serum ($n = 4$ per group). **e**, Whole-body oxygen consumption of mice ($n = 6$ per group) during day and night. **f**–**n**, Procedure to analyse the treatment effect of GSK2643943A on diet-induced obese mice (**f**). Eight-week-old male C57BL/6J mice were fed HFHS diet for 15 weeks. The mice were then assigned to 2 groups ($n = 6$ per group) and gavaged with vehicle or GSK2643943A at a dose of 0 or 30 mg kg^{-1} d^{-1} for 2 weeks. **g**, Body weight. **h**–**k**, Total cholesterol (TC) and triglycerides (TG) in liver and serum. **l**, Representative H&E staining of liver and WAT sections. Scale bars, 50 μm. **m**, Quantification of the individual adipocyte size in **l**. Sixty arbitrary adipocytes were analysed by ImageJ. **n**, Glucose tolerance test. Data are mean ± s.e.m. Two-tailed Student's *t*-test (**c**, **d**, **h**–**k**, **m**) or two-way ANOVA (**e**, **g**, **n**).

Extended Data Fig. 9s, t). Serum aspartate aminotransferase (AST), alanine aminotransferase (ALT) and creatinine concentrations were similar in both groups (Extended Data Fig. 9u–w), indicating that there was no liver or kidney toxicity. Serum levels of TNFα and the expression of macrophage markers and inflammatory markers also remained unchanged by GSK2643943A treatment (Extended Data Fig. 9x, y).

Ucp1-deficient mice did not show metabolic improvements following GSK2643943A treatment, indicating that these effects were dependent on UCP1 (Extended Data Fig. 10a–l), in line with previous findings that succinate stimulates UCP1-dependent thermogenesis[33,34]. In addition, GSK2643943A specifically reduced HMGCR levels in wild-type mouse liver (Extended Data Figs. 9r, 10m). In contrast with its effects in wild-type mice, GSK2643943A treatment did not change energy expenditure, glucose clearance or serum lipid levels in L-*Usp20*$^{-/-}$ mice (Extended Data Fig. 10n–s). Thus, GSK2643943A ameliorates metabolic diseases through inhibition of hepatic USP20 and HMGCR destabilization (Extended Data Fig. 7).

Discussion

mTORC1 is a critical nutrient sensor and organizer of energy storage after feeding. Our findings place USP20 immediately downstream of mTORC1 in promoting cholesterol synthesis. Genetic or pharmacological inhibition of USP20 abolishes this nutrient-saving mechanism and provides multiple benefits to metabolism and health. First, depletion of USP20 activity reduces cholesterol biosynthesis owing to decreased levels of HMGCR protein (Fig. 1e, f). Second, triglyceride and fatty acid levels are decreased because the endogenous LXR ligands cannot be efficiently generated, thereby decreasing expression of SREBP1c and fatty acid synthetic genes (Extended Data Fig. 4h, i). Third, USP20 inhibition markedly increases energy expenditure, at least partially through an increase in succinate concentration (Fig. 3). Notably, all the metabolic features observed in L-*Usp20*$^{-/-}$ mice can be reversed by expressing the constitutively stable HMGCR(K248R) (Extended Data Fig. 7), confirming that HMGCR is the major substrate of USP20, and accounts for the metabolic improvements resulting from *Usp20* deficiency.

The enzymatic activity of HMGCR can be inhibited by statins, the most widely prescribed cholesterol-lowering drugs. Although statins are effective in lowering blood cholesterol and treating cardiovascular disease, they prevent adipocyte browning in mice and humans by impairing adipocyte protein prenylation as well as inducing new-onset diabetes in humans[36,37]. Unlike statins, USP20 inhibition only decreases hepatic cholesterol biosynthesis in the feeding state (Figs. 1f, 4c), and basal activity of HMGCR in adipocytes should remain unaffected. Similar to statins, USP20 inhibition decreases lipid levels; however, USP20 inhibition also promotes thermogenesis, which may be beneficial for a broad range of metabolic diseases. The effects of USP20 inhibition on HMGCR promote the generation of succinate from HMG-CoA (Extended Data Fig. 8a). The molecular details of this process need further investigation. In summary, this study reveals an unexpected link from mTORC1 to HMGCR through USP20 phosphorylation. USP20 inhibition could be an effective therapy to treat metabolic disorders including cardiovascular disease, hyperlipidaemia, nonalcoholic fatty liver disease, obesity and diabetes.

Online content

Any methods, additional references, Nature Research reporting summaries, source data, extended data, supplementary information, acknowledgements, peer review information; details of author contributions and competing interests; and statements of data and code availability are available at https://doi.org/10.1038/s41586-020-2928-y.

1. Luo, J., Yang, H. & Song, B. L. Mechanisms and regulation of cholesterol homeostasis. *Nat. Rev. Mol. Cell Biol.* **21**, 225–245 (2020).
2. Repa, J. J. & Mangelsdorf, D. J. The role of orphan nuclear receptors in the regulation of cholesterol homeostasis. *Annu. Rev. Cell Dev. Biol.* **16**, 459–481 (2000).
3. Edwards, P. A., Muroya, H. & Gould, R. G. In vivo demonstration of the circadian thythm of cholesterol biosynthesis in the liver and intestine of the rat. *J. Lipid Res.* **13**, 396–401 (1972).
4. Porter, J. A., Young, K. E. & Beachy, P. A. Cholesterol modification of hedgehog signaling proteins in animal development. *Science* **274**, 255–259 (1996).
5. Xiao, X. et al. Cholesterol modification of smoothened is required for hedgehog signaling. *Mol. Cell* **66**, 154–162 (2017).
6. Hu, A. & Song, B. L. The interplay of Patched, Smoothened and cholesterol in Hedgehog signaling. *Curr. Opin. Cell Biol.* **61**, 31–38 (2019).
7. Chen, L. et al. Regulation of glucose and lipid metabolism in health and disease. *Sci. China Life Sci.* **60**, 1765–1775 (2019).
8. Goldstein, J. L. & Brown, M. S. Regulation of the mevalonate pathway. *Nature* **343**, 425–430 (1990).
9. Brown, M. S. & Goldstein, J. L. The SREBP pathway: regulation of cholesterol metabolism by proteolysis of a membrane-bound transcription factor. *Cell* **89**, 331–340 (1997).
10. DeBose-Boyd, R. A. & Ye, J. SREBPs in lipid metabolism, insulin signaling, and beyond. *Trends Biochem. Sci.* **43**, 358–368 (2018).
11. Cahill, G. F., Jr. Fuel metabolism in starvation. *Annu. Rev. Nutr.* **26**, 1–22 (2006).
12. Song, B. L., Sever, N. & DeBose-Boyd, R. A. Gp78, a membrane-anchored ubiquitin ligase, associates with Insig-1 and couples sterol-regulated ubiquitination to degradation of HMG CoA reductase. *Mol. Cell* **19**, 829–840 (2005).
13. Liu, T.-F. et al. Ablation of gp78 in liver improves hyperlipidemia and insulin resistance by inhibiting SREBP to decrease lipid biosynthesis. *Cell Metab.* **16**, 213–225 (2012).
14. Jiang, L. Y. et al. Ring finger protein 145 (RNF145) is a ubiquitin ligase for sterol-induced degradation of HMG-CoA reductase. *J. Biol. Chem.* **293**, 4047–4055 (2018).

15. Song, B.-L. & DeBose-Boyd, R. A. Ubiquitination of 3-hydroxy-3-methylglutaryl-CoA reductase in permeabilized cells mediated by cytosolic E1 and a putative membrane-bound ubiquitin ligase. *J. Biol. Chem.* **279**, 28798–28806 (2004).
16. Song, B.-L., Javitt, N. B. & DeBose-Boyd, R. A. Insig-mediated degradation of HMG CoA reductase stimulated by lanosterol, an intermediate in the synthesis of cholesterol. *Cell Metab.* **1**, 179–189 (2005).
17. Cao, J. et al. Ufd1 is a cofactor of gp78 and plays a key role in cholesterol metabolism by regulating the stability of HMG-CoA reductase. *Cell Metab.* **6**, 115–128 (2007).
18. Nijman, S. M. B. et al. A genomic and functional inventory of deubiquitinating enzymes. *Cell* **123**, 773–786 (2005).
19. Sever, N. et al. Insig-dependent ubiquitination and degradation of mammalian 3-hydroxy-3-methylglutaryl-CoA reductase stimulated by sterols and geranylgeraniol. *J. Biol. Chem.* **278**, 52479–52490 (2003).
20. Rong, S. et al. Expression of SREBP-1c requires SREBP-2-mediated generation of a sterol ligand for LXR in livers of mice. *eLife* **6**, e25015 (2017).
21. Yang, C. et al. Sterol intermediates from cholesterol biosynthetic pathway as liver X receptor ligands. *J. Biol. Chem.* **281**, 27816–27826 (2006).
22. Hillgartner, F. B., Salati, L. M. & Goodridge, A. G. Physiological and molecular mechanisms involved in nutritional regulation of fatty acid synthesis. *Physiol. Rev.* **75**, 47–76 (1995).
23. Li, S., Brown, M. S. & Goldstein, J. L. Bifurcation of insulin signaling pathway in rat liver: mTORC1 required for stimulation of lipogenesis, but not inhibition of gluconeogenesis. *Proc. Natl Acad. Sci. USA* **107**, 3441–3446 (2010).
24. Condon, K. J. & Sabatini, D. M. Nutrient regulation of mTORC1 at a glance. *J. Cell Sci.* **132**, 222570 (2019).
25. Gwinn, D. M. et al. AMPK phosphorylation of raptor mediates a metabolic checkpoint. *Mol. Cell* **30**, 214–226 (2008).
26. Inoki, K., Zhu, T. & Guan, K. L. TSC2 mediates cellular energy response to control cell growth and survival. *Cell* **115**, 577–590 (2003).
27. González, A., Hall, M. N., Lin, S. C. & Hardie, D. G. AMPK and TOR: the yin and yang of cellular nutrient sensing and growth control. *Cell Metab.* **31**, 472–492 (2020).
28. Inoki, K., Kim, J. & Guan, K. L. AMPK and mTOR in cellular energy homeostasis and drug targets. *Annu. Rev. Pharmacol. Toxicol.* **52**, 381–400 (2012).
29. Yu, Y. et al. Phosphoproteomic analysis identifies Grb10 as an mTORC1 substrate that negatively regulates insulin signaling. *Science* **332**, 1322–1326 (2011).
30. Hsu, P. P. et al. The mTOR-regulated phosphoproteome reveals a mechanism of mTORC1-mediated inhibition of growth factor signaling. *Science* **332**, 1317–1322 (2011).
31. Arnedo, M. et al. More than one HMG-CoA lyase: The classical mitochondrial enzyme plus the peroxisomal and the cytosolic ones. *Int. J. Mol. Sci.* **20**, 6124 (2019).
32. Puchalska, P. et al. Hepatocyte–macrophage acetoacetate shuttle protects against tissue fibrosis. *Cell Metab.* **29**, 383–398.e7 (2019).
33. Mills, E. L. et al. Accumulation of succinate controls activation of adipose tissue thermogenesis. *Nature* **560**, 102–106 (2018).
34. Liu, K. et al. Scd1 controls de novo beige fat biogenesis through succinate-dependent regulation of mitochondrial complex II. *Proc. Natl Acad. Sci. USA* **117**, 2462–2472 (2020).
35. Harrigan, J. A., Jacq, X., Martin, N. M. & Jackson, S. P. Deubiquitylating enzymes and drug discovery: emerging opportunities. *Nat. Rev. Drug Discov.* **17**, 57–78 (2018).
36. Paseban, M., Butler, A. E. & Sahebkar, A. Mechanisms of statin-induced new-onset diabetes. *J. Cell. Physiol.* **234**, 12551–12561 (2019).
37. Balaz, M. et al. Inhibition of mevalonate pathway prevents adipocyte browning in mice and men by affecting protein prenylation. *Cell Metab.* **29**, 901–916.e8 (2019).

Methods

Mice

Usp20-floxed mice were generated by GemPharmatech using the CRISPR–cas9 system. Cas9 mRNA, single guide RNAs (sgRNAs) and donor were co-injected into zygotes. sgRNAs directed cas9 endonuclease cleavage in intron 6–7 and intron 8–9, resulting in LoxP sites inserted into intron 6–7 and intron 8–9, respectively, by homologous recombination. To obtain liver-specific knockout mice (L-*Usp20*$^{-/-}$), the floxed *Usp20* mice were crossed with albumin-cre transgenic mice.

The mice (*Usp20*$^{KI/KI}$) harbouring the USP20(S132A/S134A) mutation were generated by CRISPR–cas9-mediated genome editing (Cyagen Biosciences). In brief, the fragment for *Usp20* guide RNA (gRNA) (GGCCGTTACCTCGAGGCTTCAGG) was inserted into the gRNA cloning vector. The S132A (TCT to GCT) and S134A (TCT to GCT) mutation sites in the donor oligo were designed and synthesized. Then, cas9 mRNA and gRNA generated by in vitro transcription and donor oligo were co-injected into fertilized eggs for *Usp20*$^{KI/KI}$ mouse production.

The mice (*Hmgcr*$^{KI/KI}$) harbouring the HMGCR(K248R) mutation were generated by CRISPR–cas9-based Extreme Genome Editing system (Beijing Biocytogen). The cas9–guide RNA (gRNA) target sequences were designed to the regions on intron 6 and intron 8 to promote DNA breaks and homologous recombination. The in vitro-transcribed nuclease cas9 mRNA, gRNA and the oligo donor carrying the desired mutation (AAA→AGA, K248→R248) were co-injected into fertilized mouse eggs. The pups were identified by PCR followed by sequence analysis using primers (HMGCR K248R-F: TTGTGTTCATGACATTCTTCCCGGC; HMGCR K248R-R: CACAAGCAAAAGCCCCCAAATACCC). The *Ucp1*$^{-/-}$ mice were generous gifts from Y. Qiu (Peking University).

Male C57BL/6J mice (6–8 weeks of age) were purchased from Center for Disease Control (CDC; Hubei, China). Littermates with genotype *Usp20*$^{fl/fl}$ were used as wild-type control for the L-*Usp20*$^{-/-}$ mice in animal studies. All mice were housed in colony cages in a pathogen-free environment with the temperature maintained at 21–23 °C and relative humidity at 50–60%, and were under a 12 h:12 h light:dark cycle. All mice had ad libitum access to standard chow diet (Research Diets, D10001) before study. For fasting and refeeding experiments, mice were divided into two groups: fasted and refed. The fasted group was fasted for 12 h, and the refed group was fasted for 12 h and then refed a high carbohydrate, low fat diet (Research Diets, D12450B) for 12 h before study. Metabolic rates were measured by a comprehensive lab animal monitoring system (CLAMS) (Columbus Instruments). Measurements of VO_2 was recorded over 2 days. The analyses were performed on a 12 h:12 h light:dark cycle at 23 °C. The HFHS diet (Research Diets, D12468) was used to develop diet-induced obesity. Body composition of mice was measured by time-domain nuclear magnetic resonance (TD-NMR) with Bruker Minispec LF50 (Bruker Optics). The rectal temperatures of the mice were determined by a rectal probe attached to a digital thermometer (Physitemp). Infrared thermal imaging was performed using an Inframetrics middle infrared camera model SC1000E (FLIR Systems). All animal care and use procedures followed the guidelines of the Institutional Animal Care and Use Committee of the Wuhan University.

Materials and plasmids

We obtained MG132, ubiquitin activating-enzyme (E1), recombinant human AQUApure di-ubiquitin chains (K6-linked, K11-linked, K27-linked, K29-linked, K33-linked, K48-linked and K63-linked), ubiquitin–AFC (Ub–AFC) and Flag–ubiquitin from Boston Biochem; dorsomorphin 2HCl (AMPK inhibitor), A-769662 (AMPK activator) and torin1 (mTOR inhibitor) from Target Molecule; wortmannin, AKT1/2 kinase inhibitor, rapamycin and GSK2643943A from Selleck Chemicals; lovastatin from Shanghai Pharm Valley; mevalonate and 25-hydroxycholesterol from Sigma; Biological grade [^{3}H]-water (100 mCi ml^{-1}, ART 0194) from American Radiolabelled Chemicals and [γ-^{32}P]-ATP (10 μCi μl^{-1}, SCP-501-150) from Hartmann Analytic. Lipoprotein-deficient serum (LPDS, density > 1.215 g ml^{-1}) was prepared from newborn calf serum by ultracentrifugation in our laboratory.

The following plasmids were constructed by standard molecular cloning technics: pCMV-HMGCR-T7 encodes full-length hamster HMGCR followed by T7 epitope tag, pCMV-INSIG1-MYC encodes human INSIG1 with a MYC epitope tag, pEF-Flag-ubiquitin encodes human ubiquitin preceded by a Flag epitope tag, pCMV-gp78-MYC encodes human gp78 followed by 5× MYC epitope, pCMV-USP20-Flag encodes human USP20 followed by 3× Flag epitope; pCMV-USP20 (C154S)-Flag, pCMV-USP20 (S132A/S134A)-Flag were mutated by Quik-Change mutagenesis. Flag-rictor, Flag-raptor, haemagglutinin (HA)–S6K and His–mAKT1(K179M) were gifts from S. Fu (Tsinghua University).

Cell culture

CHO-7, Huh-7 and HEK 293T cells were grown in a monolayer at 37 °C in 5% CO_2. Huh-7 and HEK 293T cells were maintained in DMEM containing 100 units ml^{-1} penicillin and 100 μg ml^{-1} streptomycin sulfate supplemented with 10% fetal bovine serum (FBS). CHO-7 and CHO *gp78*-KO cells were maintained in medium B (a 1:1 mixture of DMEM and Ham's F-12 medium containing 100 units ml^{-1} penicillin and 100 μg ml^{-1} streptomycin sulfate) supplemented with 5% FBS. Cholesterol depletion medium is medium B supplemented with 5% LPDS, 1 μM lovastatin, and 10 μM sodium mevalonate. Medium 199 (Life Technologies) supplemented with 5% (vol/vol) FBS, 100 units ml^{-1} penicillin and 100 μg ml^{-1} streptomycin sulfate is for primary mice hepatocytes.

Immunoblotting

Cells or tissues were collected and homogenized in the RIPA buffer (50 mM Tris-HCl, pH 8.0, 150 mM NaCl, 2 mM $MgCl_2$, 1.5% NP-40, 0.1% SDS, and 0.5% sodium deoxycholate) supplemented with protease inhibitor cocktail, 10 μM MG-132, 10 μg ml^{-1} leupeptin, 1 mM phenylmethylsulfonyl fluoride, 5 μg ml^{-1} pepstatin, 25 μg ml^{-1} *N*-acetylleucinal-leucinal-norleucinal and 1 mM dithiothreitol. The protein concentrations of lysates were determined using BCA method (Thermo Fisher Scientific). Samples were mixed with the membrane solubilization buffer (62.5 mM Tris-HCl, pH 6.8, 15% SDS, 8 M urea, 10% glycerol, and 100 mM DTT) plus the 4× loading buffer (150 mM Tris-HCl, pH 6.8, 12% SDS, 30% glycerol, 6% 2-mercaptoethanol and 0.02% bromophenol blue) and incubated for 30 min at 37 °C. The equal amounts of total proteins were resolved by SDS–PAGE and transferred to PVDF membranes. Immunoblots were blocked with 5% non-fat milk in Tris-buffered saline (TBS) containing 0.075% Tween 20 (TBST), probed with indicated primary antibodies overnight at 4 °C. After washing in TBST three times, blots were incubated with horseradish peroxidase-conjugated secondary antibodies (1:5,000) diluted in TBST supplemented with 5% skim milk for 1 h at room temperature and followed by at least 3 washes with TBST. Immunoreactivity was developed with enzymatic detection using Pierce ECL Plus western blotting substrate (Thermo Fisher Scientific).

Primary antibodies used for immunoblots were as follows: mouse monoclonal antibody against T7-tag (Merck, 69522, diluted 1:5,000), mouse monoclonal antibody P4D1 against ubiquitin (Santa Cruz, SC-8017, diluted 1:1,000), mouse monoclonal antibody (clone AC-15) against β-actin (Sigma, A1978, diluted 1:10,000) and monoclonal antibody (clone M2) against Flag-tag (Sigma, F1804, diluted 1:1,000). Mouse monoclonal antibodies (clone 9E10) against MYC-tag (diluted 1:1,000) and (clone A9) against HMGCR (diluted 1:1,000) were prepared from hybridomas (ATCC). Rabbit polyclonal antibodies against gp78 (diluted 1:1,000) and HMGCR (diluted 1:1,000) were prepared in our laboratory. Rabbit polyclonal anti-USP20 antibody (diluted 1:1,000) was purchased from Bethyl (A301-189A). Anti-phosphoserine antibody (612546) was obtained from BD Biosciences (diluted 1:1,000); anti-phospho-AMPKα (Thr172) (2535, diluted 1:1,000), phospho-mTOR (Ser2448) (5536, diluted 1:1,000), phospho-AKT (Ser473) (4060, diluted 1:1,000), phospho-4E-BP1 (Thr37/46) (2855,

diluted 1:1,000), phospho-p70 S6 kinase (Thr389) (97596, diluted 1:1,000) and phospho-acetyl-CoA carboxylase (Ser79) (11818, diluted 1:1,000), AKT (4691, diluted 1:1,000) antibodies were purchased from Cell Signaling technology. Anti-AMPKα (10929, diluted 1:1,000), mTOR (20657, diluted 1:1,000), UCP1 (23673, diluted 1:1,000), p70 S6 kinase (14485, diluted 1:1,000), ACACA (67373, diluted 1:1,000), FDFT1 (13128, diluted 1:1,000), LSS (18693, diluted 1:1,000), DHCR24 (10471, diluted 1:1,000), FASN (66591, diluted 1:1,000), 4E-BP1 (60246, diluted 1:1,000) and GAPDH (10494, diluted 1:1,000) antibodies were obtained from Proteintech. Anti-LXR alpha antibody (ab41902, diluted 1:1,000) was purchased from Abcam. Anti-LXR beta antibody (NB100-74457, diluted 1:1,000) was obtained from Novus Biologicals. Horseradish peroxidase-conjugated goat anti-mouse (115-035-003, diluted 1:5,000) and anti-rabbit (111-035-144, diluted 1:5,000) secondary antibodies were from Jackson ImmunoResearch Laboratories. Rabbit polyclonal anti-INSIG1 (diluted 1:1,000), rabbit polyclonal anti-INSIG2 (diluted 1:1,000), rabbit polyclonal anti-gp78 (diluted 1:1,000) and rabbit polyclonal anti-HMGCR (H2) (diluted 1:1,000) were prepared in our laboratory.

The rabbit polyclonal anti-phosphorylated Ser132 and Ser134 of USP20 antibodies were generated by immunizing rabbits with phosphopeptide. In brief, New Zealand white rabbits were immunized with the synthetic phosphopeptide AVPIAVADEGE(pS)E(pS)EDDDLK (corresponding to residues 121–140 of human USP20) conjugated to keyhole limpet haemocyanin. The rabbits were immunized on day 1, day 3, day 28 and day 42 and euthanized 7 days after the final immunization. The sera were collected, affinity purified with the phosphopeptide and further cleaned-up by passing through a home-made column of cyanogen bromide (CNBr)-activated sepharose 4b conjugated with non-phosphorylated peptide (AVPIAVADEGESESEDDDLK).

Immunoprecipitation

The cells were collected and suspended in 700 μl lysis buffer (0.5% Nonidet P-40, 5 mM EDTA, 5 mM EGTA in PBS) containing protease inhibitors and then passed 12 times through a 22G needle followed by centrifugation at 13,200 rpm for 10 min at 4 °C. Ninety microlitres of supernatants mixed with membrane solubilization buffer plus the 4× loading buffer as input sample. Six-hundred microlitres of supernatants were immunoprecipitated with beads conjugated with indicated antibodies at 4 °C for 6–8 h. The beads were then washed with IP buffer (0.5% Nonidet P-40, 5 mM EDTA, 5 mM EGTA in PBS) five times at 4 °C, then boiled with 2× loading buffer (75mM Tris-HCl, pH 6.8, 50mM NaCl, 6% SDS, 15% glycerol and 0.02% bromophenol blue) at 95 °C for 10 min and mixed up a solution of equal parts supernatants and HMGCR solubilization buffer. Aliquots were analysed by immunoblotting.

Preparation of mouse liver cytosol

Male mice were housed in colony cages, maintained on a 12 h:12 h light:dark cycle, and fed a chow diet. Mice were subjected to a fasting and refeeding. The mice livers were perfused with 0.9% (w/v) NaCl through the portal vein at room temperature. The livers were excised, cut into small pieces, and adjusted to 1 ml per 0.5 g liver sample with ice-cold buffer (50 mM Hepes-KOH at pH 7.2, 250 mM sucrose, 70 mM potassium acetate, 5 mM potassium EGTA and 2.5 mM magnesium acetate), plus protease inhibitors (20 μM leupeptin, 5 μg ml^{-1} pepstatin A, 25 μg ml^{-1} *N*-acetylleucinal-leucinal-norleucinal and 1 mM dithiothreitol). All subsequent steps were carried out at 4 °C. Homogenates were centrifuged at 1,000*g* for 10 min. The supernatants from this spin were subjected sequentially to centrifugation at 20,000*g* for 20 min, 186,000*g* for 1 h, and 186,000*g* for 45 min. A volume of 2 μl supernatant was taken for BCA protein quantification. The final supernatant, designated as cytosol (15–20 mg of protein ml^{-1}). The final supernatant was divided into multiple aliquots, snap-frozen in liquid nitrogen, and stored at −80 °C. For experiments, tubes were thawed in a 37 °C water bath and placed on ice until use.

Preparation of membrane fractions

On day 0, CHO-7 cells were plated onto dishes (8×10^5 cells per 10-cm dish) in 10 ml DMEM/F12 medium supplemented with 5% FBS. After incubation for 12 h at 37 °C in 5% CO_2, the attached cells were washed once with PBS and then incubated at 37 °C overnight in DMEM/F12 medium supplemented with 5% LPDS, 1 μM lovastatin and 10 μM mevalonate. After 16 h, two 10-cm dishes of cells were collected and resuspended in 500 μl buffer A (10 mM HEPES/KOH, pH 7.6, 1.5 mM $MgCl_2$, 10 mM KCl, 5 mM EDTA, 5 mM EGTA, 250 mM sucrose) with protease inhibitors as described above. The cell suspension was passed through a 22.5-gauge needle 15 times and centrifuged at 1,000*g* for 10 min at 4 °C. The supernatant was used to prepare the membrane fraction by centrifugation at 20,000*g* for 15 min at 4 °C. The pellet was designated as the membrane and stored at −80 °C.

In vitro ubiquitination of HMG-CoA reductase

The cell membrane fractions were prepared from sterol-depleted CHO cells and analysed by in vitro ubiquitination assay in a final volume of 0.3 ml of the buffer (25 mM Hepes-KOH at pH 7.3, 115 mM potassium acetate, 5 mM sodium acetate, 2.5 mM $MgCl_2$ and 0.5 mM sodium EGTA) containing the ATP-regenerating system (2 mM Hepes-KOH at pH 7.3, 1 mM magnesium acetate, 1 mM ATP, 30 mM creatine phosphate and 0.05 mg ml^{-1} creatine kinase), 0.1 mg ml^{-1} Flag–ubiquitin, 1.6 μg ml^{-1} E1, 1.6 μg ml^{-1} E2,10 μg ml^{-1} 25-HC, 10 μg ml^{-1} cholesterol and 1–10 mg ml^{-1} of protein from mouse liver cytosol. Typical reactions were carried out at 37 °C for 30 min. The reaction mixture was mixed with 300 μl 1% NP-40 buffer containing protease inhibitors as described above and passed through a needle 15 times. The solutions were centrifuged at 13,200 rpm for 10 min at 4 °C. Lysates were pre-cleared with 3 μg of normal rabbit IgG and 40 μl of protein A/G plus-agarose (sc-2003, Santa Cruz Biotechnology) for 1 h at 4 °C, followed by immunoprecipitation with 6 μg of rabbit polyclonal anti-HMGCR and 100 μl of protein A/G plus-agarose overnight at 4 °C. After washing with immunoprecipitation buffer containing protease inhibitor cocktail for five times, immunoprecipitates were eluted with 2× loading buffer at 95 °C for 10 min, and then centrifuged at 12,000 rpm for 1 min. Supernatants were then mixed with equal volume of membrane protein solubilization buffer and incubated at 37 °C for 30 min. Aliquots of the immunoprecipitates were subjected to SDS–PAGE and immunoblot analysis.

In vitro deubiquitination assay with liver cytosol

On day 0, CHO-7 cells were plated onto dishes (8×10^5 cells per 10-cm dish) in 10 ml DMEM/F12 medium supplemented with 5% FBS. After incubation for 12 h at 37 °C in 5% CO_2, the cells were washed once with PBS and then incubated at 37 °C overnight in DMEM/F12 medium supplemented with 5% LPDS, 1 μM lovastatin and 10 μM mevalonate. The sterol-depleted CHO-7 cells were then treated with or without 1 μg ml^{-1} 25-HC in the presence of 10 μM MG132 for 2 h to induce HMGCR ubiquitination. Membrane fractions were isolated from homogenates of cells and immunoprecipitated with anti-HMGCR antibody-coupled agarose. The pellet samples were then incubated with liver cytosols of fasted or refed mice for 30 min at 37 °C, and the reaction was stopped by adding loading buffer, followed by SDS–PAGE and analysis by immunoblotting.

In vitro deubiquitination assay with purified USP20

HEK 293T cells were transfected with plasmids expressing Flag-tagged wild-type USP20 or USP20(C154S). After 48 h, Flag-USP20 was immunoprecipitated with anti-Flag beads for 6 h at 4 °C. After extensive washing with buffer, the bound proteins were eluted with 3× Flag peptide. Various Ub2 molecules were incubated with purified aliquots of wild-type USP20 and USP20(C154S) in 30 μl deubiquitylation buffer (50 mM Tris-HCl pH 8.0, 150 mM NaCl, 1 mM EDTA, 5 mM dithiothreitol) for 2 h at 37 °C. After reaction, boiled with 10 μl of 4× loading buffer for 10 min and analysed by immunoblotting.

DUB activity was measured by detecting the increase in fluorescence upon cleavage of ubiquitin–AFC. Purified USP20 variants were added individually to 200 µl deubiquitinating assay buffer (50 mM Tris-HCl pH 7.4, 20 mM potassium chloride, 5 mM magnesium chloride, 1 mM DTT, including 0.5 µM ubiquitin–AFC), and incubated at 37 °C for 1 h. The fluorescence intensity was measured using a spectrometer with excitation and emission wavelengths set at 400 and 505 nm, respectively.

In vitro kinase assay

For mTORC1/2 in vitro kinase assays, USP20–Flag, HA–S6K and His–AKT1 were expressed in HEK 293T cells by transient transfection and immunopurified on anti-Flag beads, anti-HA beads and Ni-NTA beads respectively. The immunoprecipitates were dephosphorylated by incubating with 1 U μl^{-1} λ-phosphatase and 5 U ml^{-1} calf intestinal phosphatase at 30 °C for 1 h and extensively washed with NP-40 lysis buffer, followed by a final wash with kinase buffer (20 mM HEPES pH 7.4, 50 mM KCl and 10 mM $MgCl_2$). The immunoprecipitates were then aliquoted equally into six Eppendorf tubes. mTORC1/2 complexes were purified from HEK 293T cells transfected with Flag-raptor and Flag-rictor, respectively. Cells were treated with 100 nM insulin for 30 min to stimulate kinase activity. Cells were collected and lysed in lysis buffer containing 20 mM HEPES pH 7.4, 50 mM NaCl, 50 mM NaF, 10 mM β-glycerophosphate, 2 mM EDTA and 0.3% CHAPS. Clarified cell lysates were incubated with anti-Flag agarose for 2 h on ice. The beads were washed three times with lysis buffer, once with high salt lysis buffer (containing 0.5 M NaCl) and once with kinase buffer. The complexes were eluted with 0.1 mg ml^{-1} Flag peptide diluted in kinase buffer, aliquoted, incubated with or without 2 µM torin1 for 5 min, and mixed with indicated substrates. The reaction was primed with the addition of 100 µM cold ATP (or containing additional 10 µCi per tube [γ-^{32}P]ATP for autoradiography of USP20). After 30 min incubation at 30 °C with tumbling, the reaction was terminated by the addition of 1/3 volume of 4× Laemmli loading buffer. The mixture was briefly spun and loaded onto SDS–PAGE and transferred to PVDF membrane. ^{32}P-labelled USP20 was visualized by a storage phosphoscreen and a phosphoimager. S6K and AKT1 are substrates of mTORC1 and 2, respectively, and were used as controls.

Cholesterol synthesis in vivo

Mice were fasted for 12 h, or fasted for 12 h and then refed with a high-carbohydrate, low-fat diet for 12 h before study. Each animal was injected intraperitoneally with 5 mCi of [^{3}H]-water in 150 µl of isotonic saline. One hour after injection, each animal was euthanized. The liver and kidney were removed, and 200–300 mg portions were saponified, and the sterols were isolated by petroleum ether extraction. The rates of cholesterol synthesis were calculated as the [^{3}H]-water incorporated into sterols per hour per gram of tissue.

Glucose tolerance and insulin tolerance tests

Ahead of studies, mice were fasted for 16 h for glucose tolerance tests (GTT) or 4 h for insulin tolerance tests (ITT). In GTT studies, glucose (2 g kg^{-1}body weight) was injected intraperitoneally into mice. For ITT, mice received an intraperitoneal injection of insulin (0.75 U kg^{-1} body weight). Tail-blood glucose levels were measured at 0, 15, 30, 60, 90 and 120 min after challenge using the Onetouch Ultra blood glucose monitoring system (Johnson).

Blood and liver chemistry

Mouse blood was collected by retro-orbital bleeding. The livers were homogenized and supernatants were collected for lipid extraction. Total cholesterol and triglyceride levels were determined by the total cholesterol kit and triglyceride kit according to the manufacturer's instructions (Kehua Bioengineering). Free fatty acids were measured enzymatically with the LabAssay NEFA kit (294-63601, Wako). The serum level of insulin was measured by the mouse insulin immunoassay kit (MS100, EZassay). The serum levels of ALT and AST were determined according to the manufacturer's instructions (C009-2-1 for ALT, C010-2-1 for AST, NJJCBIO). Serum triiodothyronine (T_3), thyroxine (T_4), TNF, thyroid-stimulating hormone (TSH), secretin, adrenaline, noradrenaline and creatinine were measured using ELISA kits (CEA453Ge for T_3, CEA452Ge for T_4, SCA133Mu for TNF, CEA463Mu for TSH, CEB075Mu for secretin, CEA858Ge for adrenaline, CEA907Ge for noradrenaline, CEV806Ge for creatinine, Cloud Clone).

Mass spectrometric analysis of phosphopeptides

Immunoprecipitated proteins were separated by SDS–PAGE and digested by in-gel tryptic digestion. The gel slices were treated with 10 mM DTT and 55 mM iodoacetamide to reduce the disulfide bond and alkylate the resulting thiol group. Trypsin was added at a final concentration of 10 ng μl^{-1} for overnight digestion at 37 °C. The phosphopeptides were enriched by using a home-made TiO_2 microcolumn. In brief, the digested peptides were loaded in 80% acetonitrile (ACN), 5% trifluoroacetic acid (TFA), 1 M glycolic acid, washed with 80% ACN, 1% TFA and 10% ACN, 0.1% TFA, eluted with 2 M $NH_3{\cdot}H_2O$, and desalted in a R3 microcolumn. LC–MS/MS was performed using EASY-nLC 1000 system interfaced to Q Exactive HF (Thermo Scientific). The enriched phosphopeptides were loaded in solvent A (0.1% formic acid) onto a trap column and separated on an analytical column (5 µm, 100 µm internal diameter × 2 cm; 3 µm, 75 µm internal diameter × 25 cm Reprosil-Pur C18-AQ, Thermo Scientific) at a flow rate of 250 nL min^{-1} in a 60-min gradient (2–30% solvent B (0.1% fatty acids in ACN) over 48 min; 30–90% over 2 min and 90% for 10 min). For data-dependent acquisition, full-scans (m/z 300–1,800) were acquired in the orbitrap with a resolution of 60,000, and the 20 most abundant ions in each MS scan were automatically selected and fragmented at a resolution of 30,000. The raw files were searched against Uniprot homo sapiens (v2015-11-11) database using Proteome Discoverer (Thermo Scientific, v.2.1). Trypsin was chosen as the enzyme, with a maximum of two missed cleavages. Cysteine carbamidomethylation was defined as a fixed modification and variable modifications included methionine oxidation, acetylation on the N terminus and phosphorylation at serine, threonine and tyrosine residues. The precursor mass tolerance was set to 10 ppm, and the fragment mass tolerance was set to 0.02 Da. The false discovery rate (FDR), calculated on the basis of a decoy database search, was set to 1%.

Metabolomics analysis

The mice were fasted for 12 h and then refed for 6 h. Polar metabolites were extracted from liver tissues using a mixture of ACN:methanol (1:1, v/v) and analysed by ultraperformance liquid chromatography with tandem mass spectrometry (UPLC–MS/MS) conducted on a Waters Acquity UPLC-system coupled with 5500 QTRAP hybrid dual-quadrupole ion-trap mass spectrometer (SCIEX). Chromatographic separation was achieved on a Waters Acquity UPLC BEH Amide Column (2.1 × 100 mm, 1.7 µm particles) using a flow rate of 0.5 ml min^{-1} at 40 °C during a 6 min gradient (0–1 min 95% B, 1–2.5 min from 95% B to 40% B, 2.5–4.5 min 40% B, 4.5–5.0 min from 40% B–95% B, 5–6 min 95% B), using solvent A (25 mM ammonium hydroxide, 25 mM ammonium acetate, pH 9.0) and solvent B (100% acetonitrile). The mass spectrometer was operated in a polarity switching mode with electrospray source voltage set to +5,500 V in positive mode and −4,500 V in negative mode, the curtain gas was set to 35 and collision gas was set to medium (nitrogen). Multiple reaction monitoring was conducted for metabolite quantitation. Peak determination and area integration were performed using Analyst 1.7.0 (SCIEX) and SCIEX OS 1.4.0 software (SCIEX).

Quantitative PCR

Total RNA was extracted from homogenized liver or cells using Trizol Reagent (Invitrogen) following the manufacturer's instructions. Total RNA was digested by RNase-free DNase I (Promega). Synthesis of cDNA

was performed using 2 μg total RNA from each sample using M-MLV Reverse Transcriptase (Promega). Quantitative PCR (qPCR) was carried out using the Hieff qPCR SYBR Green Master Mix (Yeasen Biotech) and analysed on a Bio-Rad CFX96 apparatus (Bio-Rad). Primer sequences are listed in Supplementary Table 1.

Statistics and reproducibility

No statistical methods were specifically used to calculate the sample size. Sample size was determined based on the previous studies and literature in the field using similar experimental paradigms and to reach a minimum of at least three mice per group. No data were excluded. All statistical data are presented as mean ± s.e.m. All experiments were repeated at least twice independently with similar results. All statistical analyses were performed using GraphPad Prism 7 (GraphPad Software). All parameters were tested using unpaired two-tailed Student's *t*-test, one-way ANOVA or two-way ANOVA as described in the figure legends. A *P* value below 0.05 was considered statistically significant. Unless stated otherwise, the experiments were not randomized and investigators were not blinded to allocation during experiments. Blinding was performed in in vitro experiments and data analysis by different operators.

Reporting summary

Further information on research design is available in the Nature Research Reporting Summary linked to this paper.

Data availability

All source data for immunoblotting are shown in Supplementary Fig. 1. Source data are provided with this paper.

Acknowledgements We thank D. Liang and B.-Y. Xiang for technical assistance; Y. Qiu and S. Fu for reagents; and X. Zhou and L. Deng for bomb calorimetry. This work was supported by grants from the National Natural Science Foundation China (91957103, 91954203, 31690102 and 32021003) and Ministry of Science and Technology China (2016YFA0500100). B.-L.S. acknowledges the support from the Tencent Foundation through the Xplorer Prize.

Author contributions X.-Y.L. and X.-J.S. carried out the overall experiments and analysed the data. A.H., Y.D., and W.J. performed the screening of the DUB expression library. A.H. performed the in vitro kinase assay and in vitro deubiquitination assay. J.-Q.W. performed experiments in UCP1-knockout mice and HMGCR(K248R) knock-in mice. Y.D. and M.S. assisted with the animal and cell experiments. X.Z. performed metabolites analysis and analysed the data. B.-L.S. conceived the project and directed the research. B.-L.S., X.-Y.L., X.-J.S., W.Q. and J.L. wrote the paper with input from the other authors.

Competing interests The authors declare no competing interests.

Additional information
Supplementary information is available for this paper at https://doi.org/10.1038/s41586-020-2928-y.
Correspondence and requests for materials should be addressed to B.-L.S.
Peer review information *Nature* thanks Wayne Hancock and the other, anonymous, reviewer(s) for their contribution to the peer review of this work.
Reprints and permissions information is available at http://www.nature.com/reprints.

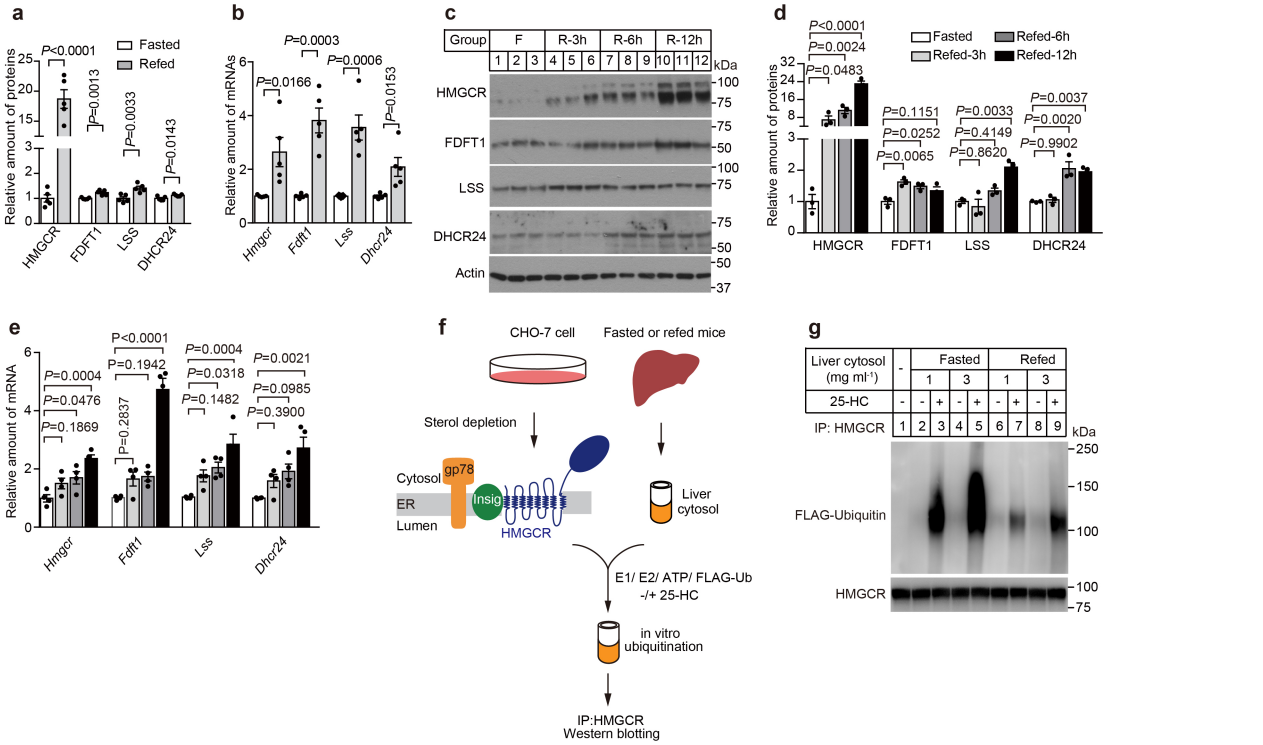

Extended Data Fig. 1 | In vitro ubiquitination assay of HMGCR. **a**, Quantification of the proteins in Fig. 1a. The signals of HMGCR, FDFT1, LSS and DHCR24 were normalized to that of GAPDH. The amount of each protein in fasted state was defined as 1. **b**, Relative amounts of mRNAs in the livers of the mice in Fig. 1**a** measured by qPCR. **c**, Immunoblot analysis of HMGCR, FDFT1, LSS and DHCR24 in the livers of mice fasted (F) for 12 h, or fasted for 12 h and then refed (R) with a high-carbohydrate/low-fat diet for 3 h, 6 h, or 12 h ($n = 3$ per group) respectively. **d**, Quantification of proteins in (**c**). **e**, The mRNA levels of indicated genes in mouse liver ($n = 4$ per group) treated as in (**c**). **f**, Schematic representation of the experimental design for in vitro ubiquitination assays. Membrane fractions were prepared from the sterol-depleted CHO-7 cells to provide un-ubiquitinated HMGCR and E3 complex. The liver cytosols were prepared from mice under fasted or refed conditions. The membrane fractions were incubated with E1, UBE2G2, ATP, FLAG-Ubiquitin, the indicated cytosol and 25-hydroxycholesterol (25-HC) at 37 °C for 30 min. Samples were solubilized and HMGCR was immunoprecipitated with polyclonal anti-HMGCR antibodies. Immunoblotting was carried out with monoclonal anti-FLAG or monoclonal anti-HMGCR antibodies. **g**, In vitro ubiquitination of HMGCR as described in (**f**). Experiments were performed as indicated three times with similar results. All values are presented as mean ± SEM. Data were analysed by unpaired two-tailed Student's *t*-test (**a**, **b**), or one-way ANOVA with Tukey's multiple comparisons test (**d**, **e**).

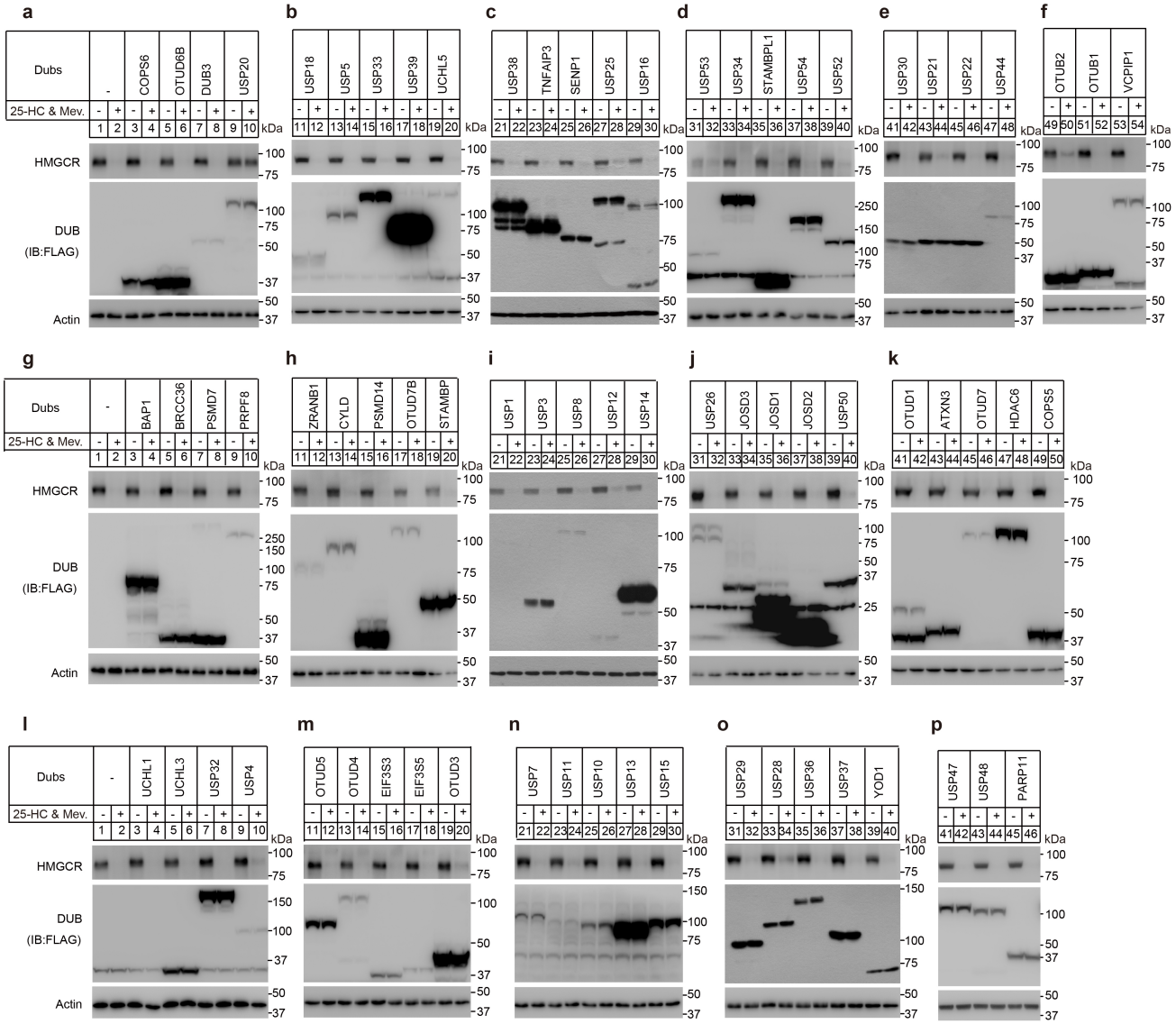

Extended Data Fig. 2 | The screening of the DUB expression library. Experiments were performed as indicated three times with similar results. **a**–**p**, CHO-7 cells were set up for experiments on day 0 at 4×10^5 cells per 60-mm dish in DMEM/F12 supplemented with 5% FBS. On day 1, cells were transfected in 3 ml of DMEM/F12 supplemented with 5% FBS containing 1 μg of pCMV-HMGCR-T7, 30 ng of pCMV-Insig-1-Myc and 0.3 μg indicated Dub. The total DNA was adjusted to 2 μg $dish^{-1}$ using pcDNA3 mock vector. Eight hours after transfection, cells were incubated in 3 ml of DMEM/F12 supplemented with 5% FBS. On day 2, cells were washed with phosphate-buffered saline (PBS) and then switched to DMEM/F12 containing 5% lipoprotein-deficient serum (LPDS), 1 μM lovastatin, and 10 μM mevalonate. After incubation for 16 h at 37 °C, the cells were treated with 1 μg ml^{-1} 25-HC plus 10 mM mevalonate as indicated. After 5 h at 37 °C, cells from 2 dishes were pooled and collected, lysed, and subjected to immunoblotting. Immunoblot analysis was carried out with anti-T7 IgG (against HMGCR) and anti-FLAG IgG (against DUBs) as described. Mev., mevalonate.

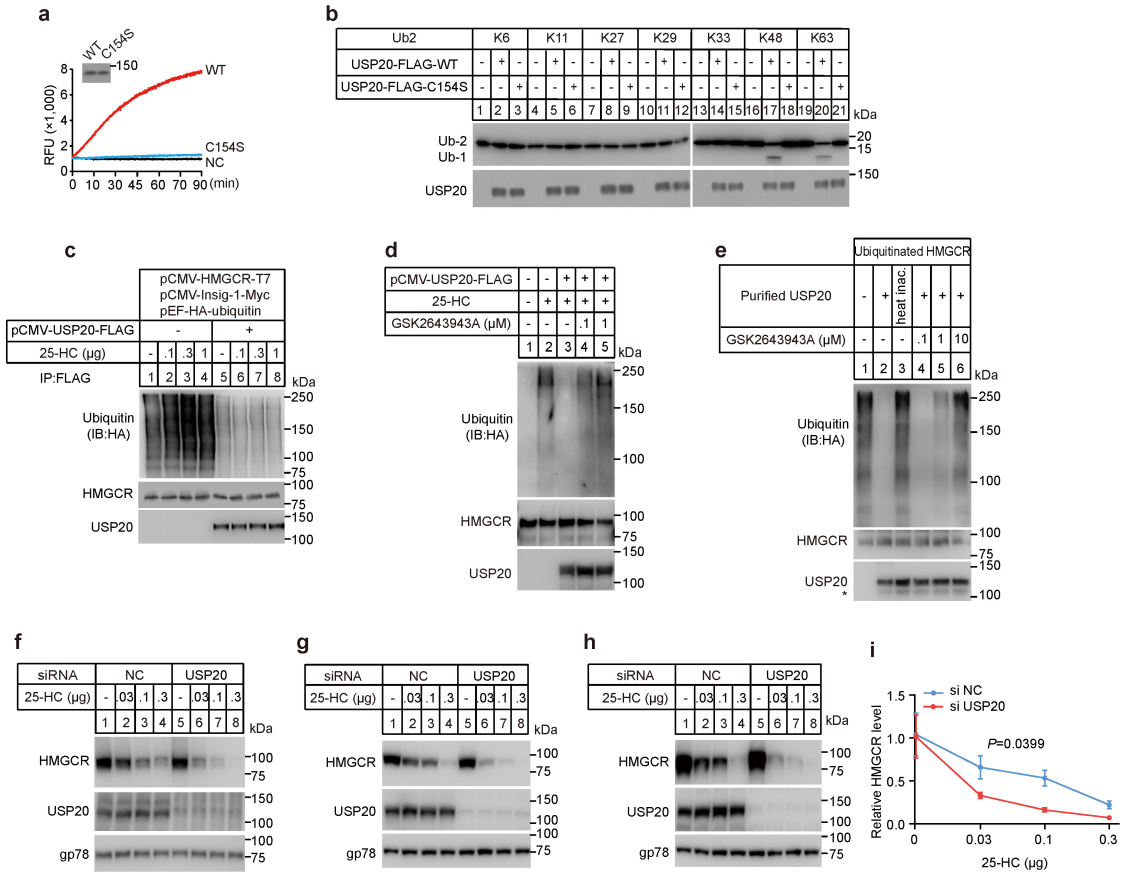

Extended Data Fig. 3 | Characterization of the deubiquitylase USP20. **a**, In vitro activities of USP20 variants indicated by the hydrolysis of a fluorogenic substrate Ubiquitin-7-amino-4-trifluoromethylcoumarin (Ub-AFC). The WT USP20 and USP20(C154S) proteins were purified from HEK 293T cells. Negative control (NC) means no protein added. Inset western blotting shows the similar amount of the proteins. **b**, Hydrolysis of various linked di-ubiquitin (Ub2) by USP20 in vitro. **c**, USP20 decreases sterol-induced ubiquitination of HMGCR. CHO-7 cells were transfected with the indicated plasmids, depleted of sterols as in Extended Data Fig. 2 and then treated with 25-HC plus 10 μM MG132 for 2 h. Cells lysates were immunoprecipitated with anti-T7 beads. The pellet was immunoblotted with anti-HA antibody and anti-HMGCR. The input was immunoblotted with anti-FLAG. **d**, GSK2643943A inhibits USP20-mediated deubiquitination of HMGCR. CHO-7 cells were transfected with plasmids and depleted of sterols. Then the cells were treated with 1 μg ml^{-1} 25-HC in the presence of MG132 for 2 h. Cell lysates were immunoprecipitated with anti-T7 beads. The pellet was immunoblotted with anti-HA and anti-HMGCR antibodies. The input was immunoblotted with anti-FLAG. **e**, GSK2643943A inhibits USP20-mediated HMGCR deubiquitination in vitro. The sterol-depleted CHO-7 cells were treated with 25-HC plus MG132. Cells lysates were immunoprecipitated with anti-HMGCR antibody-coupled agarose. The pellet samples were then incubated with recombinant USP20 protein for 30 min at 37 °C. *: non-specific band. USP20 was inactivated by boiling for 10 min as a control. Experiments in (**a**–**e**) were performed as indicated three times with similar results. **f**–**h**, Knockdown of *Usp20* accelerated sterol-induced degradation of HMGCR. Huh7 cells were transfected with scrambled (negative control, NC) or USP20-targeting siRNA, treated as in Fig. 1**d**. The experiments were repeated for three times. **i**, Quantification of HMGCR in (**f**–**h**). Data are mean ± SEM and were analysed by two-way ANOVA.

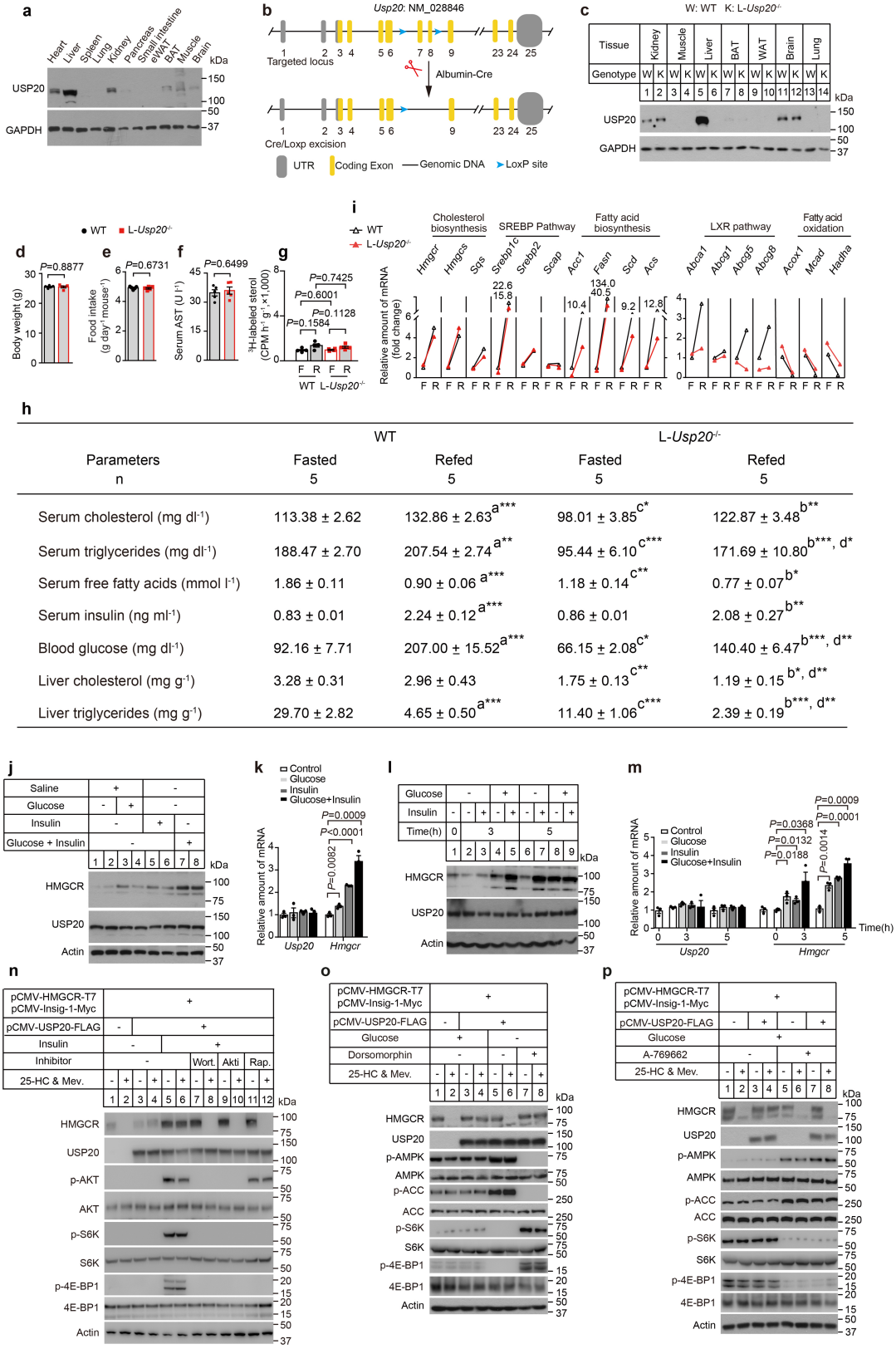

Extended Data Fig. 4 | See next page for caption.

Extended Data Fig. 4 | Characterization of L-*Usp20*$^{-/-}$ mice and the regulation of hepatic HMGCR by glucose and insulin. a, Tissue distribution of mouse USP20 protein. **b**, Schematic of L-*Usp20*$^{-/-}$ gene-targeting strategy. **c**, Immunoblotting analysis of different tissues of WT and L-*Usp20*$^{-/-}$ mice. **d**-**f**, Body weight (**d**), food intake (**e**) and serum AST (**f**) of male WT and L-*Usp20*$^{-/-}$ ($n = 5$ per group) mice fed chow diet ad libitum. **g**, Incorporation of tritium-labelled H_2O into sterol in kidney of the mice ($n = 4$ per group) as in Fig. 1**f. h**, Eight-week-old male L-*Usp20*$^{-/-}$ and their male WT littermates were fed chow diet and subjected to fasting and refeeding treatment. The metabolic parameters were measured. Each value represents mean ± SEM of data from five mice. *$P < 0.05$, **$P < 0.01$, ***$P < 0.001$ for the level of statistical significance (unpaired two-tailed Student's *t*-test) between WT and L-*Usp20*$^{-/-}$ mice under the same condition. The "a" means refed WT mice versus fasted WT mice; "b" means refed L-*Usp20*$^{-/-}$ versus fasted L-*Usp20*$^{-/-}$; "c" means fasted L-*Usp20*$^{-/-}$ versus fasted WT mice; "d" means refed L-*Usp20*$^{-/-}$ versus refed WT mice. **i**, Relative amounts of mRNAs in the livers of the mice treated as in (**h**). Each value represents mean of data from three mice. **j**, Immunoblotting analysis of hepatic HMGCR protein upon glucose and insulin stimulation. Eight-week-old male WT mice were fasted overnight and intraperitoneally injected with 2 mg g^{-1} glucose or 0.75 mU g^{-1} insulin or both. After 3 h, liver samples were subjected to immunoblotting. **k**, qPCR analysis of the mRNAs in mice livers ($n = 3$ per group) treated as in (**j**). **l**, WT mouse primary hepatocytes were untreated (-) or treated (+) with 25.5 mM glucose or 10 nM insulin for 3 h or 5 h. **m**, qPCR analysis the mouse primary hepatocytes ($n = 3$ per group) treated as in (**l**). **n**, Inhibition of mTOR signalling antagonizes insulin-induced stabilization of HMGCR. WT primary hepatocytes were grown in M199 medium. On day 1, cells were transfected plasmids and depleted of cholesterol by incubating in M199 medium containing 5% LPDS, 1 μM lovastatin and 10 μM mevalonate for 16 h. Then, the cells were switched to the same medium with indicated inhibitor (Wort. wortmannin, 0.2 μM; AKTi, AKT1/2 kinase inhibitor 10 μM; Rap. Rapamycin, 0.1 μM). After 2 h, cells were treated with or without 1 μg ml^{-1} 25-HC plus 10 mM mevalonate in the absence (-) or presence (+) of insulin and the indicated inhibitors for 5 h. Immunoblots were performed with the indicated antibodies. **o**, Effect of AMPK inhibition Dorsomorphin. WT primary hepatocytes were transfected, depleted of sterol, treated with 1 μM Dorsomorphin, 5.5 mM (-) or 25.5 mM (+) glucose combined with 1 μg ml^{-1} 25-HC plus 10 mM mevalonate for 5 h. **p**, Effect of AMPK activation A-769662. WT primary hepatocytes were transfected, depleted of sterol, treated with 1 μM AMPK activator A-769662, 25.5 mM (+) glucose combined with 1 μg ml^{-1} 25-HC plus 10 mM mevalonate for 5 h. Experiments in (**a**, **c**, **l**–**p**) were performed as indicated twice with similar results. Statistical significance was determined using unpaired two-tailed Student's *t*-test (**d**–**g**, **k**, **m**). Bars represent mean ± SEM.

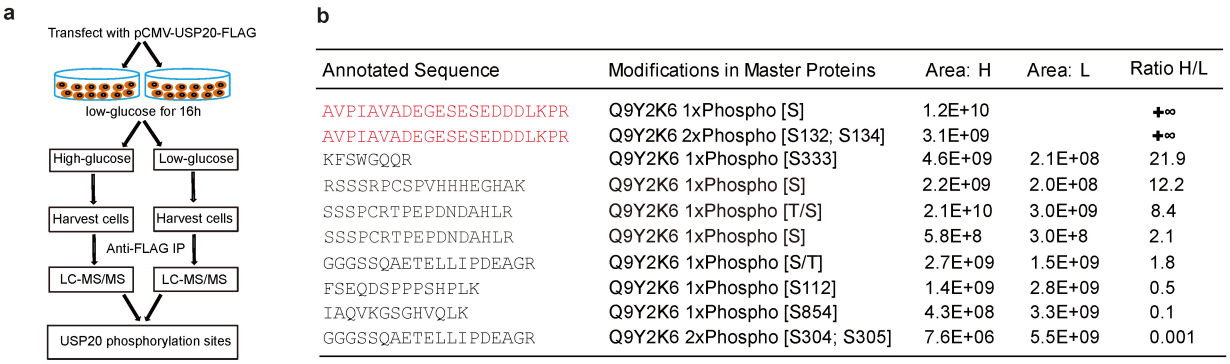

b

Annotated Sequence	Modifications in Master Proteins	Area: H	Area: L	Ratio H/L
AVPIAVADEGESESEDDDLKPR	Q9Y2K6 1xPhospho [S]	1.2E+10		+∞
AVPIAVADEGESESEDDDLKPR	Q9Y2K6 2xPhospho [S132; S134]	3.1E+09		+∞
KFSWGQQR	Q9Y2K6 1xPhospho [S333]	4.6E+09	2.1E+08	21.9
RSSSRPCSPVHHHEGHAK	Q9Y2K6 1xPhospho [S]	2.2E+09	2.0E+08	12.2
SSSPCRTPEPDNDAHLR	Q9Y2K6 1xPhospho [T/S]	2.1E+10	3.0E+09	8.4
SSSPCRTPEPDNDAHLR	Q9Y2K6 1xPhospho [S]	5.8E+8	3.0E+8	2.1
GGGSSQAETELLIPDEAGR	Q9Y2K6 1xPhospho [S/T]	2.7E+09	1.5E+09	1.8
FSEQDSPPPSHPLK	Q9Y2K6 1xPhospho [S112]	1.4E+09	2.8E+09	0.5
IAQVKGSGHVQLK	Q9Y2K6 1xPhospho [S854]	4.3E+08	3.3E+09	0.1
GGGSSQAETELLIPDEAGR	Q9Y2K6 2xPhospho [S304; S305]	7.6E+06	5.5E+09	0.001

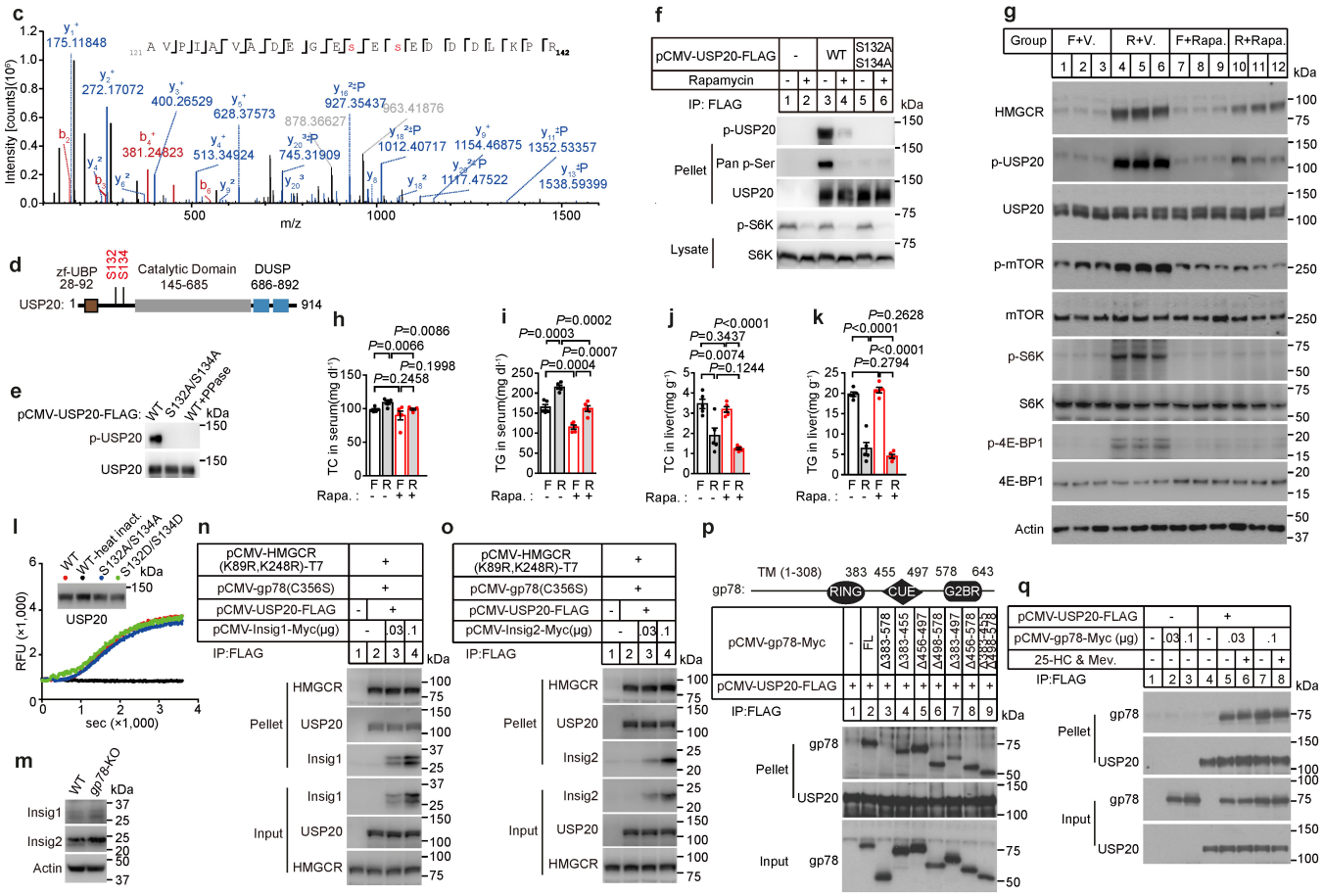

Extended Data Fig. 5 | Analysis the phosphorylation sites of USP20 and its interaction with gp78. a, Procedure to identify the phosphorylated sites of USP20. **b**, The top 10 of phosphorylated USP20 peptides. H: high glucose; L: low glucose. **c**, Mass spectrum showing that USP20 was phosphorylated at S132 and S134. **d**, Domain organization of USP20. zf-UBP: zinc-finger ubiquitin binding domain; DUSP: domain present in ubiquitin-specific protease. **e**, Validation of the home-made phospho-specific antibody recognizing p-S132/p-S134 of USP20 (p-USP20). USP20 was immunoprecipitated from HEK 293T cells, treated with or without 1U μl^{-1} λ-phosphatase and 5U ml^{-1} CIP (PPase), eluted with FLAG peptide and subjected to immunoblotting. **f**, Rapamycin attenuates USP20 phosphorylation. WT primary hepatocytes were transfected with the indicated plasmid, pre-treated with 100 nM rapamycin for 30 min, and then stimulated with 25.5 mM glucose plus 10 nM insulin for additional 1 h. Cells were lysed with 0.5% NP-40 containing protease and phosphatase inhibitors and immunoprecipitated with anti-FLAG agarose. **g**, Eight-week-old male WT mice were subjected to fasting and refeeding. Vehicle or rapamycin (5 mg kg^{-1}) were intraperitoneally injected 1 h before fasting or refeeding respectively. Immunoblot analysis of liver samples was performed. F: fasted; R: refed; V: vehicle; Rapa.: rapamycin. **h**, **i**, Serum total cholesterol (**h**) and triglyceride (**i**) of the mice in (**g**) ($n = 5$ per group). **j**, **k**, Liver total cholesterol (**j**) and triglyceride (**k**) of the mice in (**g**) ($n = 5$ per group). **l**, In vitro activities of USP20 variants. The inset demonstrated equal amounts of USP20 proteins. **m**, Immunoblot analysis of endogenous Insig-1 and 2 in WT and *gp78*-KO CHO cells. **n**, **o**, Overexpression of Insig-1 (**n**) or Insig-2 (**o**) does not block HMGCR-USP20 interaction. **p**, Mapping the region of gp78 that interacts with USP20. **q**, The interaction of gp78 and USP20 is unresponsive to 25-HC and mevalonate. Experiments in (**e**, **f**, **l**–**q**) were performed as indicated twice with similar results. All values are presented as mean ± SEM. Data were analysed by unpaired two-tailed Student's *t*-test (**h**–**k**).

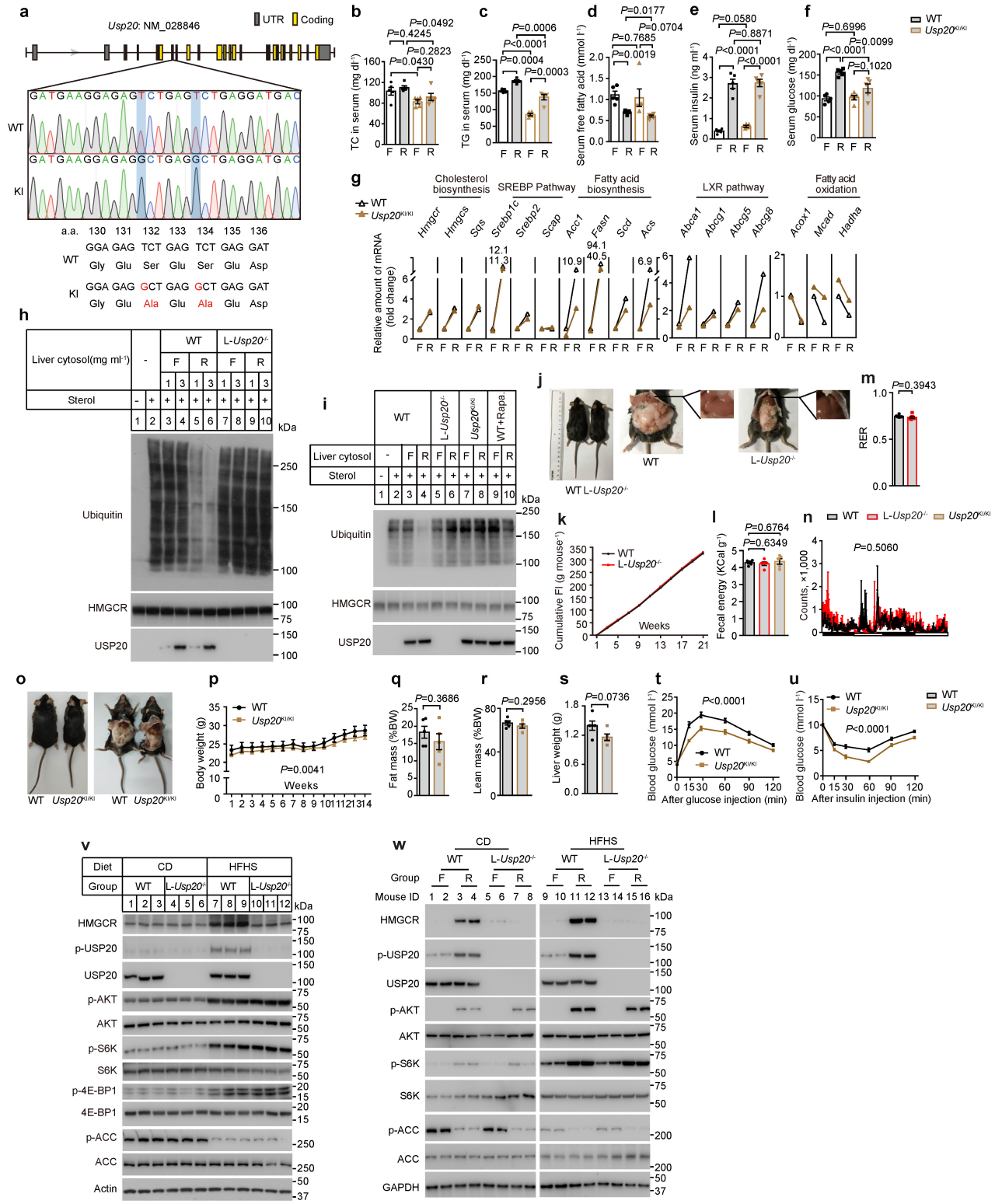

Extended Data Fig. 6 | See next page for caption.

Extended Data Fig. 6 | Characterization of the *Usp20*$^{KI/KI}$ mice and analysis the metabolism of L-*Usp20*$^{-/-}$ and *Usp20*$^{KI/KI}$ mice on HFHS. a, Strategy to generate *Usp20*$^{KI/KI}$ mice expressing USP20(S132A/S134A). **b**–**f**, Eight-week-old male *Usp20*$^{KI/KI}$ mice and their male WT littermates under chow diet were subjected to fasting and refeeding (n = 5 per group). TC (**b**), TG (**c**), free FA (**d**), insulin (**e**) and glucose (**f**) in the serum were measured. **g**, Relative amounts of mRNAs in the livers of WT and *Usp20*$^{KI/KI}$ mice subjected to fasting and refeeding treatments measured by qPCR. Each value represents mean of data from five mice. **h**, **i**, In vitro HMGCR deubiquitination assay performed as depicted in Fig. 1**b. j**–**n**, Eight-week-old male L-*Usp20*$^{-/-}$ mice and their male WT littermates were randomly grouped (n = 6 per group) and allowed ad libitum access to water and the HFHS diet for 23 weeks as in Fig. 3**a. j**, Representative image of the mice after 23-week of HFHS diet. **k**, Cumulative food intake (n = 6 per group). **l**, Measurement of fecal energy by bomb calorimetry (n = 5 per group). **m**, **n**, Respiratory exchange ratio (RER) (**m**) and movement (**n**) as determined by metabolic cages (n = 6 per group). **o**–**u**, Eight-week-old male *Usp20*$^{KI/KI}$ mice and their male WT littermates were randomly grouped (n = 5 per group) and allowed ad libitum access to water and the HFHS Diet for 14 weeks. **o**, Representative images after 14-week of HFHS diet. **p**, Body weight (n = 5 per group). **q**, **r**, Whole-body composition (n = 5 per group). **s**, Liver weight (n = 5 per group). **t**, GTT (n = 5 per group). **u**, ITT (n = 5 per group). **v**, **w**, Effect of chronic HFHS diet. Eight-week-old male L-*Usp20*$^{-/-}$ mice and their male WT littermates were randomly grouped and allowed ad libitum access to water and normal chow diet or HFHS diet for 8 weeks. **v**, Mice were fasted for 4 h and then sacrificed. **w**, Mice were subjected to fasting and refeeding treatment as in Fig. 1**a**. Liver samples were analysed by western blotting. CD: chow diet; HFHS: high-fat and high sucrose diet; F: fasted; R: refed. Each value represents mean ± SEM. Experiments in (**h**, **i**, **v**, **w**) were performed as indicated twice with similar results. Statistical significance was determined using unpaired two-tailed Student's t-test (**b**–**f**, **l**, **m**, **q**–**s**); or two-way ANOVA (**n**, **p**, **t**, **u**).

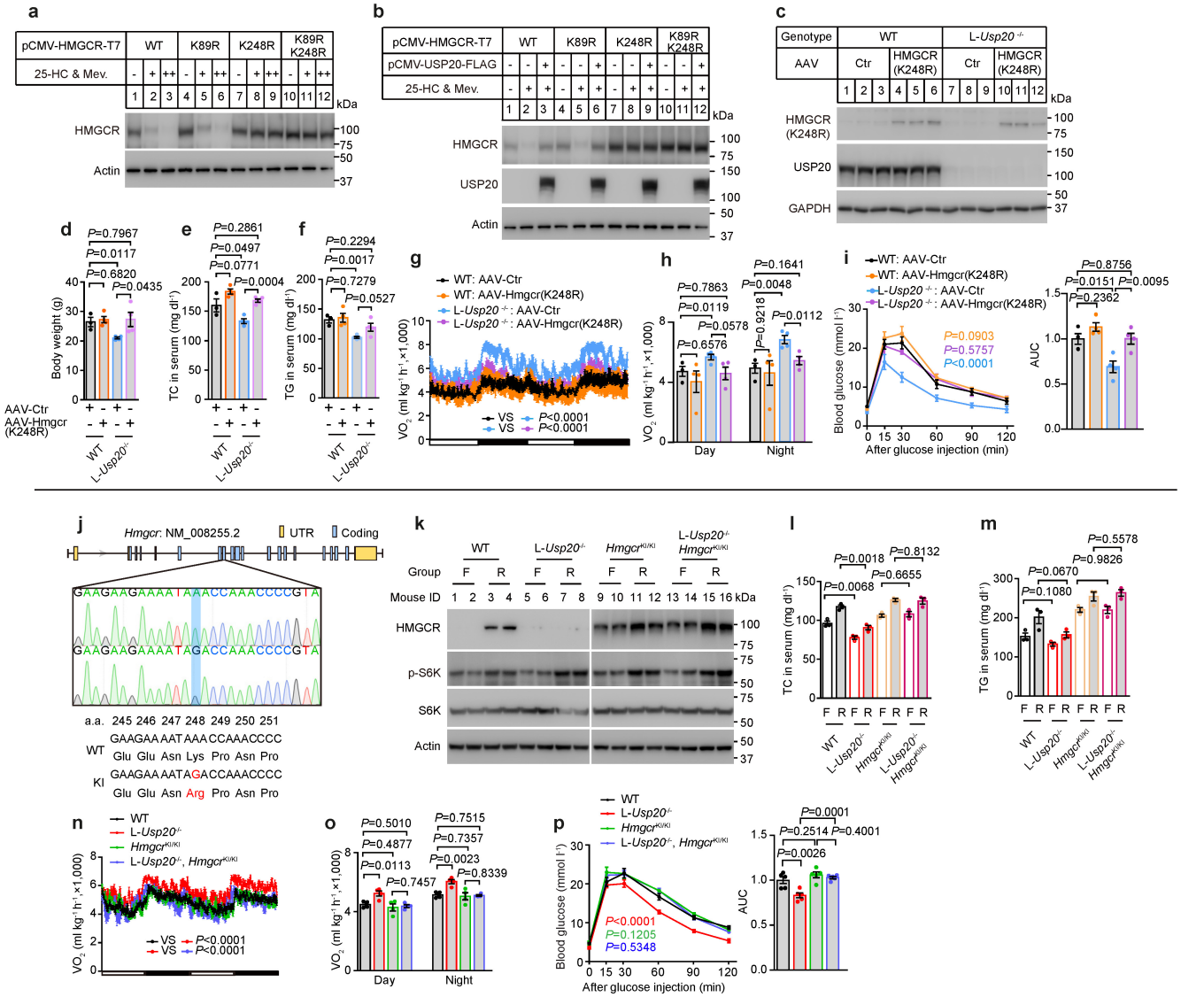

Extended Data Fig. 7 | Expression of HMGCR(K248R) by AAV or knock-in reverses the phenotypes of L-*Usp20*$^{-/-}$ mice. a, HMGCR(K248R) was resistant to sterol-induced degradation. +: 0.3 μg ml^{-1} 25-HC and 3 mM Mev; ++: 1 μg ml^{-1} 25-HC and 10 mM Mev. The experiments were carried out as described in Fig. 1**d. b**, USP20 did not increase the level of HMGCR(K248R). 1 μg ml^{-1} 25-HC and 10 mM Mev were used. **c-j**, Eight-week-old male L-*Usp20*$^{-/-}$ mice and their male WT littermates were injected with 1×10^{10} viral genome (v.g.) of AAV-HMGCR(K248R) or AAV-control (Ctr). After HFHS diet for 8 weeks, the mice were analysed. **c**, Immunoblotting analysis of liver samples. **d**, Body weight ($n = 3$ for WT injected with AAV-Ctr, $n = 4$ for other groups). **e**, Total cholesterol in serum ($n = 3$ for WT injected with AAV-Ctr, $n = 4$ for other groups). **f**, Triglyceride in serum ($n = 3$ for WT injected with AAV-Ctr, $n = 4$ for other groups). **g**, **h**, Whole-body oxygen consumption of mice over dark and light cycles ($n = 3$ for WT injected with AAV-Ctr, $n = 4$ for other groups). **i**, GTT ($n = 3$ for WT injected with AAV-Ctr, $n = 4$ for other groups). **j**, Strategy to generate *Hmgcr*$^{KI/KI}$ mice expressing HMGCR(K248R). **k**–**p**, Eight-week-old male mice were fed the HFHS diet for 7 weeks and then subjected to fasting-refeeding treatment. **k**, western blotting analysis of liver samples. **l**, Total cholesterol in serum ($n = 3$ per group). **m**, Triglyceride in serum ($n = 3$ per group). **n**, **o**, Whole-body oxygen consumption of mice ($n = 4$ per group). **p**, GTT ($n = 5$ per group). Each value represents mean ± SEM. Experiments in (**a**–**c**, **k**) were performed as indicated twice with similar results. Statistical significance was determined using unpaired two-tailed Student's *t*-test (**d**–**f**, **h**, **i** (right), **l**, **m**, **o**, **p** (right)); or two-way ANOVA (**g**, **i** (left), **n**, **p** (left)). F: fasted; R: refed.

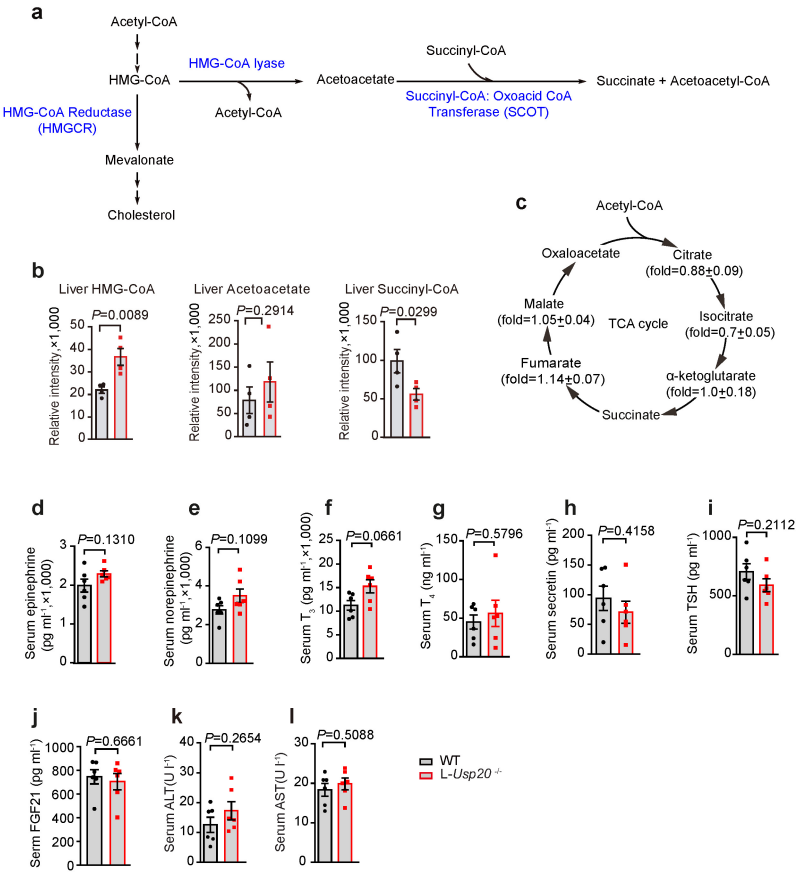

Extended Data Fig. 8 | Level of tricarboxylic acid metabolites and some factors. a, Proposed link between cholesterol biosynthetic pathway and succinate. **b**, Levels of the metabolites in liver. The male WT and L-*Usp20*$^{-/-}$ littermates ($n = 4$ per group) were fasted for 12 h and then refed for 6 h. The metabolites were measured by liquid chromatography-tandem mass spectrometry (LC-MS/MS). **c**, Changes in the metabolites associated with the tricarboxylic acid cycle in liver. The male WT and L-*Usp20*$^{-/-}$ littermates ($n = 4$ per group) were fasted for 12 h and then refed for 6 h. Liver metabolites were measured by LC-MS/MS. The fold change was calculated through dividing the L-*Usp20*$^{-/-}$ mice value by the WT mice mean value. *$P < 0.05$ for the level of statistical significance (unpaired two-tailed Student's *t*-test) between WT and L-*Usp20*$^{-/-}$ mice. **d**–**l**, The epinephrine (**d**), norepinephrine (**e**), triiodothyronine (T3) (**f**), thyroxine (T4) (**g**), secretin (**h**), thyroid-stimulating hormone (TSH) (**i**), FGF21 (**j**), ALT (**k**) and AST (**l**) of L-*Usp20*$^{-/-}$ and WT mice ($n = 6$ per group). The data were analysed by unpaired two-tailed Student's *t*-test (**b**, **d**–**l**). The values present as mean ± SEM.

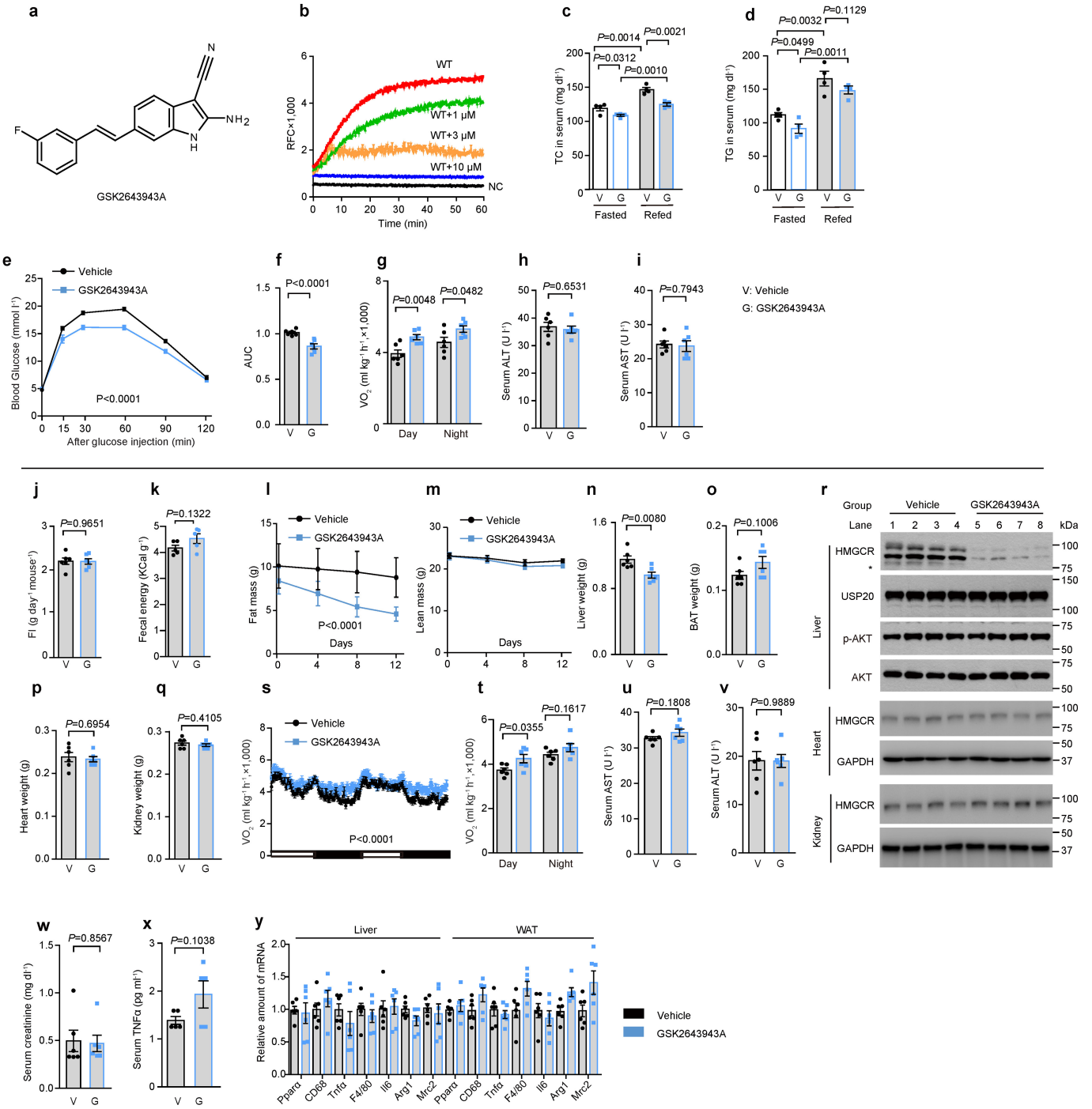

Extended Data Fig. 9 | Analysis of the mice receiving GSK2643943A. **a**, Chemical structure of GSK2643943A. **b**, In vitro deubiquitylase activity of USP20 inhibited by 1, 3, or 10 μM GSK2643943. NC: no USP20 control. **c**–**i**, The mice were treated as in Fig. 4a. TC (**c**) and TG (**d**) in serum of mice treated with vehicle (V) or GSK2643943A (G) were measured after fasting and refeeding ($n = 4$ per group). **e**, **f**, GTT ($n = 6$ per group). **g**, Quantification of whole-body oxygen consumption of mice ($n = 6$ per group) in Fig. 4e. **h**, **i**, Serum ALT (**h**) and AST (**i**) of the mice ($n = 6$ per group). **j**-**y**, The mice were treated as in Fig. 4f. **j**, Food intake ($n = 6$ per group). **k**, Measurement of fecal energy ($n = 5$ per group) by bomb calorimetry. Fat mass (**l**), lean mass (**m**) of the mice ($n = 6$ per group) measured at the indicated time. Liver weight (**n**), BAT weight (**o**), heart weight (**p**) and kidney weight (**q**) of the mice ($n = 6$ per group) measured on Day 14. **r**, On Day 14 shown in Fig. 4f, the mice were fasted for 4 h and then sacrificed. The tissue samples were analysed by western blotting. Experiments in (**r**) were performed as indicated twice with similar results. **s**, **t**, Whole-body oxygen consumption of the mice ($n = 6$ per group) measured by metabolic cages. **u**–**w**, AST (**u**), ALT (**v**) and creatinine (**w**) in serum of the mice ($n = 6$ per group). **x**, Serum TNFα ($n = 5$ per group). **y**, Expression of the genes including macrophage markers (CD68, F4/80 and Arg1) and inflammatory markers (TNFα and IL6) of the mice ($n = 6$ per group) determined by qPCR. All values are expressed as means ± SEM. Data were analysed by two-way ANOVA (**e**, **l**, **s**), or unpaired two-tailed Student's *t*-test (**c**, **d**, **f**–**k**, **n**–**q**, **t**–**y**).

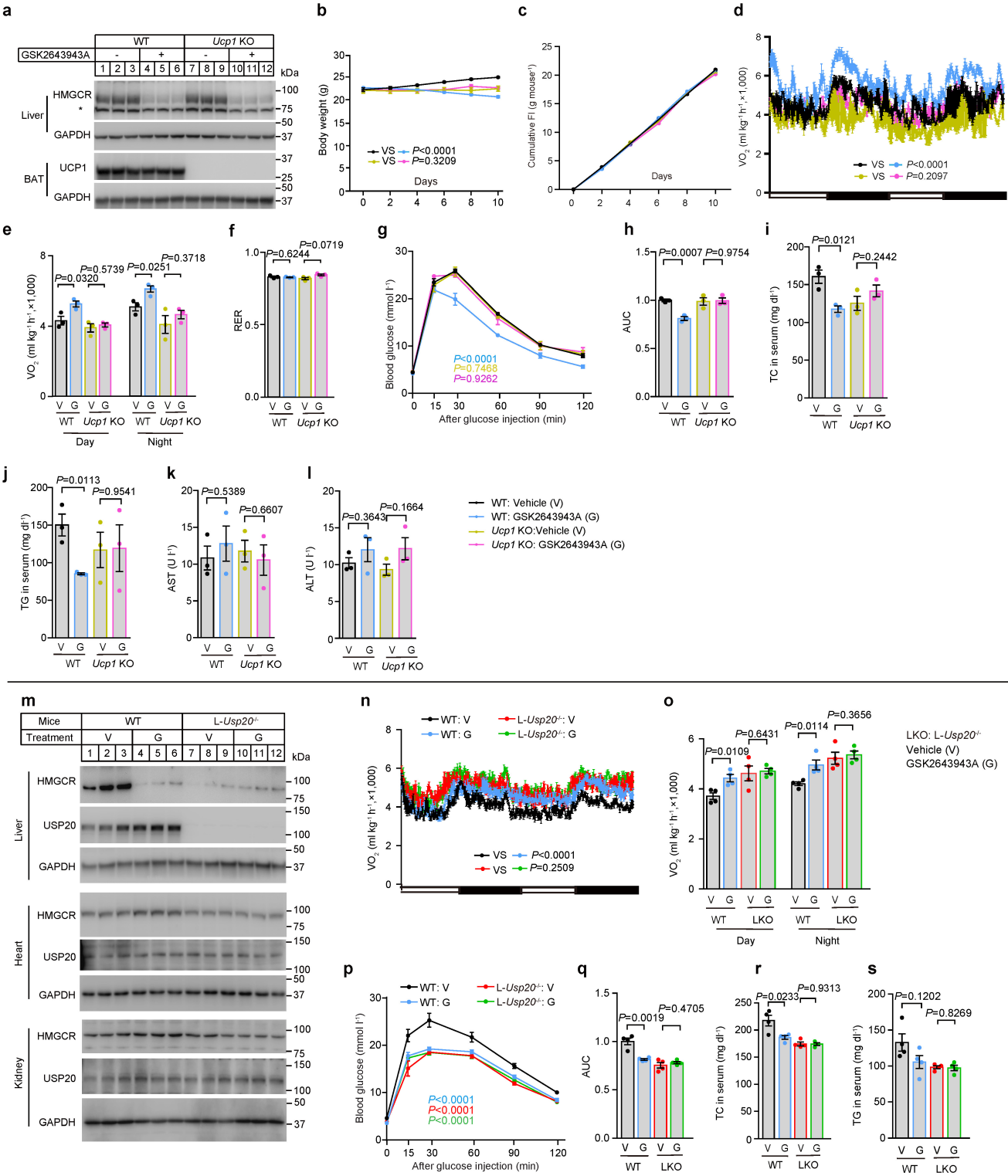

Extended Data Fig. 10 | Analysis the effects of GSK2643943A on *Ucp1* KO or L-*Usp20*$^{-/-}$ mice. a–**l**, Eight-week-old male *Ucp1* KO mice and their male WT littermates were randomly grouped, fed the HFHS diet and gavaged with vehicle or 30 mg kg^{-1} GSK2643943A daily for 13 days. GTT and metabolic cage analysis were performed on day 7 and 10, respectively. **a**, Immunoblotting analysis. *: non-specific band. **b**, Body weight per mouse ($n = 3$ per group) during the experiments. **c**, Cumulative food intake for each treatment. Each value represents mean of data from three mice. **d**, **e**, Whole-body oxygen consumption of the mice ($n = 3$ per group) measured by metabolic cages. **f**, Respiratory exchange ratio (RER) over dark and light cycles ($n = 3$ per group). **g**, **h**, GTT analysis ($n = 3$ per group). **i**–**l**, TC (**i**), TG (**j**), AST (**k**), and ALT (**l**) in the serum ($n = 3$ per group). **m**–**s**, Eight-week-old male L-*Usp20*$^{-/-}$ mice and their male WT littermates were randomly grouped, fed the HFHS diet and gavaged with vehicle or 30 mg kg^{-1} GSK2643943A daily for 13 days. GTT and metabolic cage analysis were performed on day 7 and 10, respectively. **m**, Immunoblotting analysis. **n**, **o**, Whole-body oxygen consumption of the mice ($n = 4$ per group) measured by metabolic cages. **p**, **q**, GTT analysis ($n = 4$ per group). **r**, Total cholesterol in serum ($n = 4$ per group). **s**, Triglyceride in serum ($n = 4$ per group). All values are expressed as means ± SEM. Experiments in (**a**, **m**) were performed as indicated twice with similar results. Data were analysed by unpaired two-tailed Student's *t*-test (**e**, **f**, **h**–**l**, **o**, **q**–**s**), or two-way ANOVA (**b**, **d**, **g**, **n**, **p**).